Numerical Simulation of Fire Exposed Facades - An intitial investigation

Carlsson, Jörgen; Karlsson, Björn

2001

Numerical Simulation of Fire Exposed Facades

-An initial investigation

Jörgen Carlsson, Björn Karlsson

Department of Fire Safety Engineering
Lund University, Sweden

Brandteknik
Lunds tekniska högskola
Lunds universitet

Report 3123, Lund 2001

Rapporten har finansierats av Nordic Wood

Numerical Simulation of Fire Exposed Facades

-An initial investigation

Jörgen Carlsson
Björn Karlsson

Lund 2001

Numerical Simulation of Fire Exposed Facades - An initial investigation

Jörgen Carlsson, Björn Karlsson

ISSN: 1402-3504
ISRN: LUTVDG/TVBB--3123--SE

Number of pages: 82
Illustrations: Jörgen Carlsson

Keywords
CFD, Numerical simulation, Flame spread, Fire growth, Facades.

Sökord
CFD, Numerisk simulering av brand, Flamspridning, Brandtillväxt, Fasader.

Abstract
The aim of this report is to describe the fundamental physics employed in Computational Fluid Dynamics and how this can be used to predict the exposure of a facade. Simulations have been carried out for a full-scale scenario, the SP Fire 105 experiments and an intermediate scale test series recently performed by VTT, Finland. The primary objective has been to evaluate how well a CFD code can produce quantitative reliable results in terms of facade surface temperatures, gas phase temperatures and total heat flux. For the considered scenarios it is shown that the performance of the discrete transfer radiation model (DTRM) is quite insensitive to the number of prescribed rays. The gas phase models show good agreement with all test data.

Brandteknik
Lunds tekniska högskola
Lunds universitet
Box 118
221 00 Lund

brand@brand.lth.se
http://www.brand.lth.se

Telefon: 046 - 222 73 60
Telefax: 046 - 222 46 12

Department of Fire Safety Engineering
Lund University
P.O. Box 118
SE-221 00 Lund
Sweden

brand@brand.lth.se
http://www.brand.lth.se/english

Telephone: +46 46 222 73 60
Fax: +46 46 222 46 12

Summary

Performing full-scale fire experiments requires plenty of time, considerable preparation and a lot of money. As being the most direct and a visually appealing method this way has traditionally been the only way to go in many areas including facade and interior lining examination. It is not probable that full-scale experiments can be replaced, at least not in a near future, but what if the engineer could make qualified estimations on the outcome from the experiments? For example, this would mean that the number of costly full scale tests could be reduced to a minimum and that the engineer and architect together could feel more free in using different facade claddings from given criteria. This would also be consistent with the performance based building regulations. But with the performance-based regulations, demands on well-defined methods will rise.

During the last decades Computational Fluid Dynamics, CFD, has been used in many disciplines for example aerodynamics, combustion science, for weather predictions and for various design purposes. Also, a growing fire engineering society has become a potential user. CFD computer models tend to require lots of computer power and traditionally these models have been run using super computers. However, recent programming efforts, increasing CPU and memory speed and capacity have made these codes accessible for ordinary personal computers. Nevertheless, it should be pointed out that running a CFD code is still relatively expensive in terms of time, user knowledge and computer power.

The purpose of this initial work has been to investigate and, if possible, to establish a ground for using CFD methodology as a complement or a substitute to full scale experiments. Thus, in a fire safety design situation including combustible facade materials, allowing the building constructor an environmentally and technically appealing tool for assessing different building materials.

Flame spread is rather complex as phenomenon and its modelling is one of today's most challenging research frontiers in fire science. As the thermal radiation is believed to be the single parameter having the largest influence on the spread of flame in real fire situations, this work has focused on applied radiation modelling and the effect of incident radiative flux on primarily non-combustible facades.

The discrete transfer radiation model has been used, with prescribed rays varying between 16 to 256. A too few number of rays has been reported to result in numerical errors, in both time and space (distribution). Particularly, when using an inappropriate set of prescribed rays in the standard discrete transfer radiation model numerical errors known as "ray effects" may lead to discrepancies and non-physical results. Nevertheless, the ray-effect did not cause any considerable errors and in the scenarios simulated it seems as if the number of prescribed rays can be as low as 16 without causing more than about 5% deviation from the simulations using a higher ray distribution. One reason for this is believed to be connected with the even fire-source that characterises both simulated scenarios. From the same reason, the numerical discrepancies can increase as the flame spread model is implemented, given that the fire growth is unevenly distributed on the combustible wall. From the simulations it was especially noted that the radiation model need to be called several times per time step even though the calculation does converge perfectly well at the first occasion. A correct simulation of radiative heat fluxes will be highly dependent upon the solution of the equations connected with the turbulent reacting flow as well as radiative properties of combustion gases and soot and the discretisation of the spherical solid angle.

The radiation calculations, in this work using the DT radiation model, are very demanding in terms of computer power/CPU time and their capability to make sound predictions has been proved somewhat indecisive for large scale calculations using up to 256 rays. In general, a high number of rays do not seem to be justified by calculation results and a maximum number of 64 rays are recommended in similar calculations. The gas phase is predicted within the known margin of error for all scenarios.

Fire is a highly dynamic phenomenon and as such measured variables can experience significant fluctuations. Hence it is essential that, when performing experimental studies on flame spread, radiative heat fluxes be measured at several locations on the surface. This will allow for more extensive and qualitative evaluation of the performance of a flame-spread model.

Sammanfattning (Summary in Swedish)

Att utföra storskaliga fasadexperment kräver stora resurser i termer av tid, kompetens, förberedelser och pengar. Eftersom det inte funnits, och egentligen ännu inte finns, något annat verktyg för att bedömma fasaders och beklädnaders egenskaper har utförandet av olika experimentserier varit och är det enda möjliga tillvägagångssättet. Genom att utföra försök erhålls utöver tillgänglig mätdata konkret och visuellt tilltalande ”bevis” på hur ett visst material beter sig vid värmepåverkan. Det är inte sannolikt att olika beräkningsverktyg helt kan ersätta dessa experimentserier. Vad som däremot är önskvärt är en uppsättning metoder som i förväg tillåter ingenjören att värdera olika försök och på så sätt kunna göra en mer eller mindre grov utsållning av överflödiga experimentserier i ett tidigt stadium. Sådana verkyg skulle också göra det möjligt för ingenjörer att utifrån givna kriterier utvärdera hur brandsäkerheten påverkas för olika fasad- eller ytskiktsmaterial. Dessa utgångspunkter är helt i linje med de svenska funktionsbaserade byggreglerna.

Under de senare decennierna har avancerade beräkningar inom aerodynamik, meteorologi, turbulent förbränning i motorer, turbiner mm kunnat utföras med användning av CFD, Computational Fluid Dynamics. Även inom brandteknik har CFD på kort tid erhållit en särställning som simuleringsverkyg. Dylika beräkningar kräver dock relativt stora resurser i datorkraft och har traditionellt använt särskilda arbetsstationer eller superdatorer. Det är senare års snabba utveckling av CPUs och primärminnen som tillsammans med adekvat programmeringsteknik tillåtit en allt större skara användare. Trots detta är de flesta CFD koder fortfarande mycket krävande i termer av datorkapacitet, tid och användarkunskap.

Syftet med detta pilotprojekt har varit att undersöka möjligheterna för att använda CFD koden SOFIE, Simulation Of Fire In Enclosures, som komplement och ersättning till utförandet av försöksserier. På några års sikt bör finnas ett miljömässigt och tekniskt attraktivt verktyg, eller uppsättning av olika metoder med olika sofistikeringsgrad och användningsområden, som tillåter projektering i enlighet med de funktionsbaserade byggreglerna.

Flamspridning på trämaterial är en relativt komplicerad process och försök att med olika modeller simulera dess inverkan i olika brandfall är en betydande forskningsfront inom brandteknik. Vertikal och horisontell flamspridning skiljer sig fenomenologiskt åt beroende på att olika typer av värmeflöde dominerar. I uppåtriktad, vertikal, spridning dominerar termisk strålning som värmekälla medan den horisontella eller nedåtriktade flamspridningen styrs av konduktion i gasfasen. Den verikala spridningen är betydligt snabbare än horisonella och i detta projekt studerades framförallt värmeflödespåverkan mot obrännbara material då en korrekt simulering av denna parameter är avgörande för hur en inkorporerad flamspridningsmodell kan förväntas prestera.

I litteraturen finns rapporterat att en alltför grov eller otillräckligt utnyttjande av en strålningsmodell i beräkningarna kan ge upphov till felprediktioner. I detta arbete har en strålningsmodell kallad DTRM (Discrete Transfer Radiation Model) använts och antalet förutbestämda strålar har varierats mellan 16 och 256. Om ett alltför litet antal strålar används kan numeriska fel, s.k. ”ray effects” ge upphov till felaktig distribution av strålningsvärmet i rummet med ofysikaliska resultat som följd. I detta arbete kunde inte noteras någon nämnvärt inverkan av ray-effects, detta kan delvis vara beroende av att brandkällan i båda simulerade scenarier är relativt homogen över testföremålets bredd. Detta innebär att felprediktionen blir större om flamspridning implementeras och förbränningen blir ojämn. Det kan noteras att strålningsmodellen behöver anropas flera gånger varje tidssteg, ett minimum 3-5 gånger borde användas. Dessutom förutsätts en

tillfredsställande lösning av den turbulenta förbränningen och brandgasflödena samt någon form av sotmodell, samtliga av nämnda fenomen är idag föremål för avancerad forskning. Av de utförda simuleringarna har framgått att strålningsmodellen måste anropas flera gånger under varje tidssteg. Detta även om beräkningen konvergerar bra redan vid första anropet.

De strålningsmodeller som idag finns tillgängliga är mycket krävande i termer av datorkraft och deras förmåga att korrekt prediktera termisk strålning har visats vara begränsad för stora beräkningar. Generellt kan sägas att ett så stort antal strålar som 128 eller 256 inte kan motiveras utifrån numeriska resultat. Simuleringar med 16 strålar gav i de flesta fall inte mer än 5% differens jämfört med övriga fall varför ett maximalt antal av 64 strålar rekommenderas för dylika simuleringar. Gasfasen predikteras genomgående inom felmarginalerna vid jämförelse med experimentella data. En optimal implementering av DTRM liksom en hög upplösning på beräkningsgriden är avgörande för en bra simulering.

Det är av största vikt att utförandet av experimentserier sker med stor noggrannhet och att loggning av olika parametrar sker på flera platser inom försökets domän. Brand är ett högst dynamiskt fenomen och den termiska påverkan varierar högst avsevärt med tiden och även i rummet, genomtänkta försök möjliggör dock omfattande, både kvantitativt och kvalitativt, utvärdering av olika modeller.

Nomenclature

c_p	specific heat capacity at constant pressure,
f	mixture fraction,
h_{total}	total enthalpy,
k	turbulent kinetic energy,
k_a	gas absorption coefficient,
k_s	scattering coefficient,
m	mass,
$\boldsymbol{n}$	normalised vector,
p	pressure,
$\dot{q}_j^R$	heat flux due to thermal radiation,
s	stoichiometric fuel to oxidant ratio,
t	time,
t_p	dummy variable of integration,
u, v, w	gas velocity in x- y- and z- direction respectively,
u_{char}	characteristic velocity,
u_i	gas velocity in x_i direction,
$\overline{u}$	Reynolds averaged velocity,
$\widetilde{u}$	Favre averaged velocity,
u_i'	fluctuating part of gas velocity in i direction,
u_i''	fluctuating part of gas velocity i direction,
x, y, z	room co-ordinates,
x_{char}	characteristic length scale of flow,
y_{flame}	height of flame,
y_{py}	height of pyrolysis front,
$y_{py,0}$	initial height of pyrolysis front,
A	Arrhenius pre-exponential factor for a chemical reaction,
B_i	body forces in the x_i direction,
C_R, C'_R	empirical constants,
$C_{\varepsilon 1}$	empirical constant in the k-ε turbulence model,
$C_{\varepsilon 2}$	empirical constant in the k-ε turbulence model,
$C_{\varepsilon 3}$	empirical constant in the k-ε turbulence model,
C_μ	empirical constant in the k-ε turbulence model,
D	mass diffusion coefficient,
D	diffusion conductance per unit area,
E	total emissive power,
E_a	activation energy,
E_g	emissive power for a gas with temperature T_g,
F	force,
F	convective mass flux through a unit area,
G_B	buoyancy term,
G_K	shear stress term in equation,
H_r	heat of reaction,
I	radiant intensity,
K	constant in non-linear flame length correlation,
L	turbulent mixing lenght,
M_i	chemical symbol for species i,
N	number of chemical species in a reaction,
P	probability,
R	ideal gas constant,
Re	Reynolds number,

R_f flux Richardson number,
R_{fu} rate of reaction,
S_α source term in the chemical species conservation equation,
S sectional area,
T temperature,
W width of flame,
Y_α mole fraction of species α,

β thermal expansion coefficient in the k-ε turbulence model,
Γ_ϕ turbulent diffusivity for scalar ϕ,
δ Kronecker's delta,
ε viscous dissipation rate of turbulent kinetic energy,
ε emissivity,
λ heat conductivity,
μ dynamic viscosity,
μ' bulk viscosity,
μ_t turbulent kinematic viscosity,
ν kinematic viscosity,
ν_i' stoichiometric coefficient for reactant i,
ν_i'' stoichiometric coefficient for product i,
ρ density,
σ Stefan Boltzmann constant,
σ_ε turbulent Prandtl number for dissipation of turbulent kinetic energy,
σ_k turbulent Prandtl number for turbulent kinetic energy,
σ_t turbulent Prandtl number,
τ_{ij} stress tensor,
ϕ symbolises an arbitrarily scalar,
Ω arbitrarily volume in space,

Superscripts

a, b, c model constants in the Arrhenius expression for the rate of reaction,
$'$ Reynolds averaged fluctuating variable,
$''$ Favre averaged fluctuating variable,
$\cdot$ time derivate,
– Reynolds, or time, average,
~ Favre, or density weighted, average.

Subscripts

α arbitrary chemical species,
fu fuel or fuel stream,
i, j, k Cartesian co-ordinator directions,
Nb neighbouring control volume,
ox oxidant or oxidant stream,
pr products,
py pyrolysis,
t turbulent,
vir virgin material,
vol volatiles,

Table of contents

1. Background

In today's building codes the use of wooden facades are restricted in all Nordic countries. Conducting full-scale flammability tests of facade materials can make it possible for the building designer to be more generous in the use of wood instead of other perhaps less aesthetic non-combustible materials. These full-scale experiments are however, very costly, and as representing the only currently available method, not very attractive.

However, during the last decade there has been a world-wide move towards replacing prescriptive regulations by performance criteria and performance design procedures with respect to fire risks in buildings. At the same time there has been a rapid progress in the development of models for predicting flame spread and fire growth on combustible materials. These methods are of various degrees of sophistication and complexity. Some give approximate answers for specified end-use scenarios, can be used by non-experts and require simple input. Others are more general, but may require expert knowledge and large amount of non-standard input data.

This part concerns the use of computational techniques in evaluating the impact on facade claddings from a fire. Full-scale experiments simulating postflashover fire as well as intermediate scale tests are considered. Experimental results, using both combustible and non-combustible facade materials, are available from SP, Sweden (SP-Fire 105), and from VTT Finland.

In this study only the Swedish, SP tests were simulated in full scale. The Finnish full-scale test rig uses wooden cribs and particleboard as primary fire load in the combustion chamber whereas the Swedish test uses heptane. Whilst the former has the advantage of representing a somewhat more natural and authentic fire load the latter fuel is better defined and thus more readily applied in modelling and computational terms.

To complement the large-scale tests, simulations of intermediate scale experiments are carried out in this work, allowing the use of a higher numerical resolution in the CFD code.

By performing calculations using a non-combustible facade cladding a calibration simulation is obtained. This is of great importance since it will lay a foundation for future work and also acting as a validation scenario. Thus, giving advise on how to choose input parameters, what models to use under these circumstances and pointing out the weak parts both concerning the general application of CFD and governing parameters for the development of fire growth models.

At present, no international standard test method or test criteria are available. However an ISO project is running with this very intention. In the meantime national building regulations and full-scale tests are used.

1.1 Acknowledgements

This work has been financed by Nordic Wood, a research- and development program initiated by the Nordic Industrial Fund and financed by the Nordic wood industry.

2. The Swedish building code, BBR

The Swedish building regulations have been performance based since 1994. As regards facades and facade claddings, the regulations state that the construction and composition shall be such that it does not contribute to the production of smoke and heat in a way that can jeopardise safe escape and efficient fire-fighting or represent a danger to people in the vicinity [1].

Four performance criteria that are to be fulfilled by a facade in a building class Br 1 are specified (BBR 5:631):

- The fire compartmentation is to be intact.
- Fire spread inside and on the outside of the external wall is to be limited with regard to the function of the building and the fire fighting possibilities.
- The risk for fire spread through window is to be limited.
- Parts of the facade are not to fall down.

In the general recommendation, added to this regulation, it is stated that facade cladding of wooden panel or material with a certain, prescribed, ignition resistance comply with the requirements if:

1. The building has only two floors
2. The cladding, regardless of the number of floors, covers only the ground floor.
3. Measurements are taken to ensure that the overall fire safety of the building is not reduced (such as installation of automatic sprinkler etc).

Regardless of the cladding used in the facade construction, a minimum vertical distance of 1.2 meters between windows in different fire compartments is further recommended. This is a recommendation based upon tradition and applies for all geometrical shapes and dimensions of windows. It does not consider the actual thermal influence from a fire, which will vary considerably depending on the size and shape of the opening, the fuel etc.

The general advice also states that a facade construction tested according to the full-scale test procedure SP Fire 105 and approved in accordance with “Boverkets allmänna råd 1993:2” (Building Regulations: General advice) [2] should be considered to comply with the requirements.

In BBR 5:633 it is stated that the performance of outer walls and roof claddings for buildings with different heights shall be designed so that fast fire spread from the attic of the lower part to another fire compartment above the attic is prevented. The lower building may or may not be part of the higher building.

2.1 The SP Fire 105 test method

SP Fire 105 simulates a flashover fire on the ground floor of a three-storey building. The test-rig used in the full-scale test is illustrated in Appendix A [3]. A light-weight-concrete wall is used when testing a facade cladding, thus representing the external wall on which the cladding is normally mounted. In the case of an external wall assembly the test specimen is mounted directly on the test rig. In this work CFD simulations have been carried out for the former case, with a non-combustible surface, see chapter 6.

The opening factor for the fire compartment has not been closely examined but is within the interval 0.08 - 0.12 $m^{1/2}$ and the ratio between opening height and width is quite low in the test. This will make the fire plume to move close to the facade and will likely result

in a larger heat flux than would have been obtained for an opening of square shape. A tall window could be expected to project the flames away from the building.

As fire source, a tray of 60-litre heptane is used corresponding to a fire load of approximately 75 MJ/m^2. The rate of heat release as function of time is shown in Appendix B, [3]. Integrating this curve over time reveals that the RHR presented is actually too low. This discrepancy is primarily believed to be linked to incomplete combustion, measuring errors and that the hood does not collect all of the combustion gases. The hood capacity was approximately 22-23 m^3/s, which should be compared with the maximum mass flow in the smoke plume, which can be approximated to 40 m^3/s (based on max RHR from opening factor).

2.2 Acceptance criteria for SP Fire 105 test method

The present acceptance criteria for a specimen tested according to SP Fire 105 originate from Ondrus and Pettersson [4] and are stated in "Boverkets Allmänna råd 1993:2" [2]. Two cases are taken into account, buildings with up to eight-storeys and building with more than eight storeys including all health care facilities.

1. For buildings up to eight-storey height that allow external fire fighting considering the equipment available to the local Fire Department (except for health care facilities):

    a) Parts of the facade are not to fall down in large pieces, endangering the safe escape from the building and also the safety of fire fighting personnel.

    b) Fire spread is not to reach further than to the lower part of the window two storeys above the room of fire origin.

    c) Fire is not to spread to the eaves two storeys above the room of fire origin.
    The numerical equivalent to this is assumed to be a limiting gas temperature of 500 °C for no more than two minutes and 450 °C for more than ten minutes measured at the eaves.

2. For buildings more than eight-storeys high, health care facilities and buildings up to eight storeys high which do not allow effective fire fighting from the outside:

    a), b) and c) as above

    d) The facade is not to enhance the risk for vertical fire spread to any other fire compartment. The numerical equivalent to this criterion is assumed to be a limit of 80 kW/m^2 heat flux into the centre of the window in the first storey above the room of fire origin.

Alternative acceptance criteria have been further developed by Östman et al [5]. For example a limit on the heat flux two storeys above the fire was added as presented in table 2.1.

Table 2.1.

Criteria	**Acceptance limit**
Falling pieces	< 0.1 m^2 No burning droplets
Heat flux[1]	< 80 kW/m^2 one storey above room of fire origin < 20 kW/m^2 two storeys above room of fire origin
Fire spread	< eaves

[1] The limiting heat fluxes should be read considering that untreated wood will ignite at an incident heat flux of 13 kW/m^2 given the presence of a pilot flame.

The fire-spread criterion has been modified to include protection of the attic only, and does not specify any maximum height for flame spread or charring. In order to make this criterion computationally attractive using simple engineering approaches as well as approaches derived from first principles, a limiting value on variables such as maximum allowed temperature and/or thermal heat flux is required.

Flame spread over the front surface of a facade is believed to be reasonably straightforward to simulate using advanced flame spread models although the exact engineering methodology is still to be developed. However, flame spread on the rear side of the facade, in the ventilation cavity will be more difficult to predict due to the small dimensions. A well-disposed approach for considering this is desirable.

It can be questioned whether a limiting heat flux should be complemented with time dependence or not. Hakkarainen et al [6] propose a maximum acceptable continuous heat flux <20 kW/m^2 during one minute to the centre of a window two storeys above room of fire origin. It is argued that such a criterion covers the possibility of temporary peaks in heat flux with does not imply significant risk of additional and unacceptable fire spread. In either case, this criterion is rather straightforward from a computational point of view.

The present acceptance criterion concerning falling pieces from a facade is based on subjective rather then objective evaluation. The proposed limiting size of falling pieces from the facade of 0.1 m^2 may be held as a maximum until otherwise proven.

In association to this, flaming/burning droplets falling from the facade may have to be considered. It should be realised that flaming droplets do not occur in facades entirely made of wood. Hakkarainen [6] propose a maximum flaming droplet or debris of 0.5 m^2 in contrast to the criteria from Östman [5] where no falling droplets are permitted.

Solid pieces or droplets falling from a facade due to thermal impact are linked to specific mechanical behaviour of materials and design solutions and it is not practically viable to theoretically simulate such behaviour.

3. Fundamental physics and modelling approaches in CFD

In (deterministic) computer modelling of fires, the zone model has been and still is most widely used. The reason for this is that it is simple, easy to use and that its major drawbacks are well known and well documented from numerous, independently performed research projects.

The typical zone model divides a given volume into two separate control volumes. One upper control volume near the ceiling called upper layer, consisting of burnt and entrained hot gases and one cold lower layer which contains fresh air. In some models a smoke plume appears as a third zone. The basis of the calculations is empirical and/or semi empirical transport equations for mass, momentum, energy and chemical species.

Even though they are frequently employed, sometimes outside the range of applicability and even beyond completely understood and explored physics, these models are simplified and not suited for more complicated scenarios and scenarios where more quantitative accurate results are preferred.

In CFD simulations, often referred to as field model simulations, the simulated volume is divided into a large number of small control volumes. The number of sub-volumes is normally in an order of 10^5-10^6.

CFD (Computational Fluid Dynamics) is applied to numerically solve a set of non-linear partial differential equations derived from basic laws of nature. As these equations are somewhat too complex to be solved directly for most real flows, some simplifications and submodels, such as turbulence models for the prediction of buoyancy driven turbulent flow, combustion models and radiation models for thermal radiation etc, have to be incorporated into the computer code.

The large number of control volumes and the complexity in calculations make simulations using CFD a costly process in terms of time and computer power. The gain however, is a higher accuracy and a large number of output data from every control volume within the computational domain.

It is clear that the outcome of a CFD simulation is to a high degree dependent on the physical models that are employed and also on the numerical solution methods used. Basic knowledge on these issues can be proven to be fundamental to the final results. Therefore, this chapter summarises some of the basic theory of CFD and introduces the concept of models being used in this work, beginning with the basic principle of nature, the laws of conservation.

3.1 Governing equations of fluid flow

The governing equations are derived from the basic laws of physics. These laws are the so-called laws of conservation according to which nature remains constant with the passage of time. Mathematically the laws of conservation are usually expressed in terms of partial differential equations.

Each of the conservation equations uses a physical quantity as its dependent variable. These dependent variables are usually expressed on a unit mass basis, for example specific heat and velocity (momentum). It should be emphasised that temperature, which is a frequently used dependent variable, is not a specific property, however it arises from equations that are more basic, using specific internal energy or specific enthalpy as the dependent variable.

3.1.1 Conservation of mass

The mass conservation equation, also called the mass continuity equation or simply the continuity equation, implies that matter can be neither created nor destroyed and that the total mass in an isolated system is left unchanged regardless of the changes in physical and chemical properties of substances within the system.

Using cartesian tensor notation (where i, j and k denotes directions in a cartesian coordinate system) the differential equation is written:

$$\frac{\partial \rho}{\partial t} + \frac{\partial}{\partial x_j}(\rho u_j) = 0 \qquad \text{(Eq 3.1)}$$

I II

Here

I is the rate of change of density, or mass per unit volume, accumulation in the control volume due to density variations, and

II is the net rate of flow through the control volume due to convection

3.1.2 Conservation of momentum

Momentum is a quantity equal to the mass of an object, for example a control volume of a fluid, multiplied by its velocity. In view of that, momentum is a vector quantity.

According to Newton's second law of motion the sum of all forces acting on an object equals the time rate of change of momentum, or:

$$\frac{d}{dt}(m\boldsymbol{v}) = \sum F \qquad \textit{(Eq 3.2)}$$

Here $\boldsymbol{\Sigma F}$ is the sum of all forces acting on the object, m is the mass and $\boldsymbol{v}$ is the velocity vector. In deriving the equation for momentum conservation this relationship is always the staring point.

The law of momentum conservation implies that, in an isolated system, motion never changes and thus the total momentum remains constant in time.

The differential equation can be written:

$$\frac{\partial}{\partial t}(\rho u_i) + \frac{\partial}{\partial x_j}(\rho u_j u_i) = -\frac{\partial p}{\partial x_i} + \frac{\partial \tau_{ij}}{\partial x_j} + \rho B_i \qquad \textit{(Eq. 3.3)}$$

I II III IV V

I is the local rate of change of momentum in time for a control volume,

II is the rate of change of momentum due to motion through an unsteady flow field,

III represents pressure forces acting on the fluid,

IV are viscous shearing forces and

V represents body forces, such as gravitational forces.

As discussed earlier all terms are written on an unit volume basis and it can be seen that the left hand side represents the total change of momentum for the fluid and the right hand side include all forces acting on the fluid, this can be compared to equation 3.2.

The stress tensor, τ_{ij}, can in a general matrix form be written as:

$$\tau_{ij} = \begin{bmatrix} \tau_{11} & \tau_{12} & \tau_{13} \\ \tau_{21} & \tau_{22} & \tau_{23} \\ \tau_{31} & \tau_{32} & \tau_{33} \end{bmatrix}$$

and is determined using the relationship

$$\tau_{ij} = \left(\mu' - \frac{2}{3}\mu \right) \frac{\partial u_k}{\partial x_k} \delta_{ij} + \mu \left(\frac{\partial u_i}{\partial x_j} + \frac{\partial u_j}{\partial x_i} \right) \qquad \textit{(Eq. 3.4)}$$

Here μ is the dynamic viscosity, also called first viscosity, and μ' represent the bulk viscosity of the fluid.
The bulk viscosity has been shown to be negligible for monatomic gas mixtures and in common practise it is always set equal to zero [7].

δ_{ij} is the so-called Kronecker´s delta (identity tensor) defined as

$$\delta_{ij} = \begin{cases} 1 & i = j \\ 0 & i \neq j \end{cases}$$

Sometimes the stress tensor also includes the pressure term. The relationship is then written as

$$\sigma_{ij} = \begin{bmatrix} \sigma_{11} & \tau_{12} & \tau_{13} \\ \tau_{21} & \sigma_{22} & \tau_{23} \\ \tau_{31} & \tau_{32} & \sigma_{33} \end{bmatrix} = -p\delta_{ij} + \tau_{ij} \qquad \textit{(Eq. 3.5)}$$

The momentum conservation equations are also generally known as the Navier- Stoke equations.

3.1.3 Conservation of energy

The law of energy conservation is virtually identical to the first law of thermodynamics and it simply implies that energy can be neither created nor destroyed. Nevertheless, it can be changed from one “form” to another, including for example chemical energy, kinetic energy, potential energy et cetera.

In a multi-component reacting system, there are several mechanisms that contribute to the total heat flux, the most common known as conduction, convection and radiation. Mainly two additional effects are encountered in the literature; these are the effect of mechanical work done on the system due to buoyancy and the so-called Dufor effect. The latter describes the heat flux in a system due to concentration gradients and in general, this term can be neglected. Due to the low velocities involved in a fire the flow work term can be ignored as well [7].

The energy equation can be written in different ways depending on which quantity is used as the dependent variable. Using the total enthalpy, $h_{total}=c_pT+\Sigma Y_\alpha H_r$ where H_r is the component heat of reaction, as dependent variable, the conservation of energy equation becomes:

$$\underbrace{\frac{\partial}{\partial t}(\rho h)}_{\text{I}} + \underbrace{\frac{\partial}{\partial x_j}(\rho u_j h)}_{\text{II}} = \underbrace{\frac{\partial p}{\partial t}}_{\text{III}} + \underbrace{\frac{\partial}{\partial x_j}\left(\frac{\lambda}{c_p}\frac{\partial h}{\partial x_j} - \dot{q}_j^{\,R}\right)}_{\text{IV}} \qquad \textit{(Eq. 3.6)}$$

where h is the static enthalpy of the mixture and

I is the time rate of change of storage of enthalpy in a fluid,

II is the net rate of influx of enthalpy due to convection,

III represents the work done on the fluid due to pressure and

IV includes terms for the net flux of heat due to conduction and thermal radiation respectively.

3.1.4 Conservation of chemical species

In an ordinary fluid-flow situation the equations above can be used to describe the motion of fluids and, if relevant, the transport of heat. However, in dealing with combustion an additional conservation equation arises, that for conservation of chemical species. The relationship is used as a supplement to the mass continuity equation and it simply states that chemical species in a reacting system are conserved. This implies that the time rate of accumulation of a specific species α in a control volume must equal the net rate of flow through the volume and the net rate of production within the volume.

Considering the generalised single chemical reaction

$$\sum_{\alpha=1}^{N} \nu'_{\alpha} M_{\alpha} \leftrightarrow \sum_{\alpha=1}^{N} \nu''_{\alpha} M_{\alpha} \qquad \textit{(Eq. 3.7)}$$

where

ν_{α}' is the stoichiometric coefficient of the reactants,

ν_{α}'' is the stoichiometric coefficient of the products,

M_{α} is the chemical symbol for species α, and

N is the number of species present in the reaction.

Now because of the law of conservation of chemical species, once a value of ν_{α}' has been set there is a constraint on the values of ν_{α}'', that is ν_{α}'' cannot be arbitrary. In terms of partial differential equations the conservation of species α can be written as

$$\frac{\partial}{\partial t}(\rho Y_{\alpha}) + \frac{\partial}{\partial x_j}(\rho u_j Y_{\alpha}) = \frac{\partial}{\partial x_j}\left(\rho D \frac{\partial Y_{\alpha}}{\partial x_j}\right) + S_{\alpha} \qquad \textit{(Eq. 3.8)}$$

I II III IV

Here

I is the rate of change of α, or the accumulation of α within the control volume,

II is the net rate of influx of species α due to convection,

III is the net rate of change of α due to molecular diffusion, and

IV is the rate of change of species α due to different sources within the control volume, i.e. the net change of α from production and consumption in the control volume.

3.1.5 Equation of state

In order to close the above set of equations an equation of state is required, that is an additional equation relating relevant variables to each other is needed in order to obtain as many equations as there are unknown quantities.

For example, using ρ and T as state variables and assuming ideal gas we have:

$$p=\rho RT \qquad \textit{(Eq. 3.9)}$$

This is the ideal-gas equation.

3.1.6 Summary

The principle of conservation is one of the most fundamental features of nature. It is noted that the mathematical descriptions of conservation all have similar structures. The differential equations all contain one term for the time rate of change of the dependent variable, one term describing property change due to macroscopic movement in space (or convection) and one term representing transport due to microscopic movement (or diffusion). Thus for an arbitrary dependent variable φ a generalised conservation equation can be written as

$$\frac{\partial}{\partial t}(\rho\phi)+\frac{\partial}{\partial x_i}(\rho u_j\phi)=\frac{\partial}{\partial x_i}\left(\Gamma_{ij}\frac{\partial\phi}{\partial x_j}\right)+S_\phi \qquad \textit{(Eq. 3.10)}$$

I II III IV

where

I is the time rate of change of ϕ in the control volume,

II is the change of ϕ due to convection,

III is the change of ϕ due to diffusion and

IV is a source term.

3.2. Modelling turbulence

3.2.1 The phenomenon of turbulence

The conservation equations as presented in section 3.1 are only applicable in the case of laminar flow, i.e. in a flow characterised by a smooth and orderly motion. However, it is no secret that in practice this is generally not the case in fluid flow. Instead, most flows encountered in real life seems to be more or less irregular and random in both time and space, or to put it in other words: fluid motion is most often turbulent.

Turbulence can be characterised by the use of Reynolds number, a dimensionless number defined as the ratio of inertia forces to viscous forces.

$$\mathrm{Re} = \frac{u_{char} x_{char} \rho}{\mu} = \frac{u_{char} x_{char}}{\nu} = \frac{inertia\ \ forces}{viscous\ \ forces} \qquad \textit{(Eq. 3.11)}$$

Here

u_{char} is the characteristic velocity, usually taken as the mean velocity of the flow,

x_{char} denotes the characteristic length scale of the mean flow,

ρ is the density, and

μ and ν are the dynamic and kinematic viscosity respectively.

For a low Reynolds number, fluid motion is essentially steady and smooth and the flow is said to be laminar. Increasing the Reynolds number a transition stage will be reached where the inertia forces in the fluid dominate over viscosity to an extent where flow becomes unstable and oscillation of the flow parameters about a mean value can be observed. At high Re flow will be turbulent containing eddies, or vortices in a very large spectrum of sizes; in a fire typically ranging from sizes about the magnitude of the plume diameter to extremely small lengths where viscosity dominates over inertia, typically in an order of 1-10 micron at the so-called Kolmogorov length scale. [8].

The large scale eddies are created by whatever process driving the flow. In a fire, for example, the driving force and so the process behind the generation of large eddies, is the buoyancy. The interaction between the large scale eddies cause them to break down forming smaller eddies, and so starting a process that continues ultimately to eddy-sizes where the flow is dominated by viscosity. Due to the viscosity forces the energy in these smallest eddies will be dissipated into heat and what is called “the turbulent cascade” ends. The transition of turbulent kinetic energy through mechanical energy into thermal energy (heat) is illustrated below in *Figure 3.1*. [9]. This will be further discussed in the chapter on combustion modelling, section 3.5.

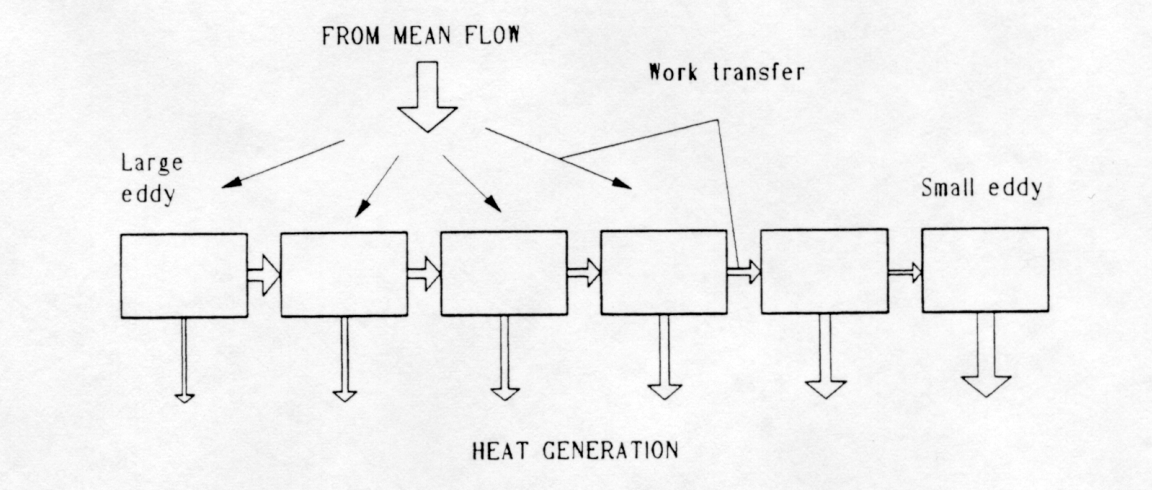

Figure 3.1 Turbulence energy transfer. [9]

Although turbulence is characterised by spatial and temporal irregularity and randomness, the turbulent motion must follow the fundamental laws of nature, the laws of conservation. However, due to these characteristic features of turbulence the computational results will necessarily be random in both time and space. This is sometimes referred to as an example of deterministic chaos. [10]

One logical way to take account for turbulence is to solve the conservation equations in such a manner that the rapid fluctuations of variables followed by turbulence can be determined. Such an approach is classified as a *Direct Numerical Simulation* (DNS) method. Using this approach in predicting turbulence the size of the control volumes needs to be consistent with the size of the smallest eddies making this method rather useless in fire modelling and other engineering usage for the time being and in a near future.

A similar technique to Direct Numerical Simulation is the *Large Eddy Simulation* (LES) method, in which the spatial resolution is made small enough to cover the largest eddies whilst an additional turbulence model is incorporated in order to take account for the smaller eddies. Similar to the DNS approach, this method is very demanding in terms of computational power and it is of limited value for the engineer. However, it becomes increasingly attractive as computer power increases, although its use in fire safety design does not belong to the near future.

From this short presentation and discussion on Direct Numerical Simulation and Large Eddy Simulation it is apparent that a simple but stable and relatively non-demanding way of modelling turbulence is desirable, particularly for engineering purposes. Nevertheless, it is interesting to note that the possibility of solving the conservation equations exactly exists. The problem is more a question of computational hardware. [11, 12]

Using the so-called Boussinesq eddy viscosity concept, the task of the turbulence model has been reduced to the determination of one single constant: the eddy viscosity μ_t. The most popular and widespread model for predicting the value of μ_t is, today, the k-ε model. [7]

3.2.2 The k-ε turbulence model

Instead of solving the turbulence directly a turbulence model can be applied to relate the fluctuating correlation of flow to the variables of mean flow using a collection of empirically derived constants. In order to do this, some simplifications has to be done. First, the governing equations are rewritten using the assumption that the instantaneous turbulent flow can be approximated as a sum between a mean and a fluctuating component.

$$u_j(x_j,t) \equiv \tilde{u}_j(t) + u_j''(x_j,t) = \frac{\overline{\rho u}_j}{\bar{\rho}} + u_j''$$

Using density-weighted averaging (time averaging for pressure and density):

Mass continuity equation:

$$\frac{\partial \bar{\rho}}{\partial t} + \frac{\partial}{\partial x_j}\left(\bar{\rho}\tilde{u}_j\right) = 0 \qquad \textit{(Eq. 3.12)}$$

Momentum conservation equation:

$$\frac{\partial \bar{\rho}\tilde{u}_i}{dt} + \frac{\partial}{\partial x_j}\left(\bar{\rho}\tilde{u}_i\tilde{u}_j\right) = -\frac{\partial \bar{p}}{\partial x_i} + \frac{\partial}{\partial x_j}\left(\bar{\tau}_{ij} - \bar{\rho}\overline{u_i''u_j''}\right) + \bar{B}_i \qquad \textit{(Eq. 3.13)}$$

Energy conservation equation:

$$\frac{\partial}{\partial t}\left(\bar{\rho}\tilde{h}\right) + \frac{\partial}{\partial x_j}\left(\bar{\rho}\tilde{u}_j\tilde{h}\right) = \frac{\partial \bar{p}}{\partial t} + \frac{\partial}{\partial x_j}\left(\frac{\lambda}{c_p}\frac{\partial \tilde{h}}{\partial x_j} - \bar{\rho}\overline{u_j''h''}\right) - \frac{\partial \overline{\dot{q}_j^R}}{\partial x_j} \qquad \textit{(Eq. 3.14)}$$

Species conservation equation:

$$\frac{\partial}{\partial t}\left(\bar{\rho}\tilde{Y}_\alpha\right) + \frac{\partial}{\partial x_j}\left(\bar{\rho}\bar{u}_j\tilde{Y}_\alpha\right) = \frac{\partial}{\partial x_j}\left(\bar{\rho}D\frac{\partial \tilde{Y}_\alpha}{\partial x_j} - \bar{\rho}\overline{u_j''Y_\alpha''}\right) + \bar{S}_\alpha \qquad \textit{(Eq. 3.15)}$$

Equation of state:

$$\bar{p} = R\sum_{\alpha=1}^{N}\left(\bar{\rho}\tilde{T}\tilde{Y}_\alpha + \bar{\rho}'\tilde{T}''\tilde{Y}_\alpha''\right)\frac{1}{M_\alpha} \qquad \textit{(Eq. 3.16)}$$

Using (an extended) Boussinesq approach the turbulent stresses in Eq 3.13 are assumed proportional to the mean velocity gradient, the mean rate of deformation, Equation 3.17. [13] [14]

$$-\bar{\rho}\overline{u_i''u_j''} = \mu_t\left(\frac{\partial \tilde{u}_i}{\partial x_j} + \frac{\partial \tilde{u}_j}{\partial x_i}\right) - \frac{2}{3}\delta_{ij}\left(\bar{\rho}\tilde{k} + \mu_t\frac{\partial \tilde{u}_k}{\partial x_k}\right) \qquad \textit{(Eq. 3.17)}$$

Here μ_t is the eddy viscosity and k is the turbulent kinetic energy, using density-weight-averaged quantities, defined as

$$\tilde{k} = \frac{1}{2}\frac{\overline{\rho u_i'' u_i''}}{\overline{\rho}} = \frac{1}{2}\overline{u_i''^2} \qquad \textit{(Eq. 3.18)}$$

One of the major assumptions used here is that the eddy viscosity is taken to be isotropic, that is the ratio between Reynolds stresses and the mean rate of deformation is identical in all directions.

This is analogous to the treatment of the laminar viscous shear stresses (Equation 3.4) with the proportionality constant, the laminar viscosity, replaced for the eddy or turbulent viscosity. However, unlike the laminar viscosity the eddy viscosity is by definition a property of the flow, not of the fluid.

Analogous to the treatment of turbulent momentum transport, turbulent scalar transport, such as energy and chemical species, can be assumed proportional to the relevant mean scalar gradient. For the density-weight-averaged scalar ϕ, the following is believed to hold

$$-\overline{\rho u_i'' \phi_j''} = \frac{\mu_t}{\sigma_t}\frac{\partial \tilde{\phi}_j}{\partial x_i} = \Gamma_\phi \frac{\partial \tilde{\phi}_j}{\partial x_i} \qquad \textit{(Eq. 3.19)}$$

Here σ_t is an empirical constant called turbulent Prandtl/Schmidt number and

$\Gamma_\phi = \frac{\mu_t}{\sigma_t}$ is known as the eddy or turbulent diffusivity for the scalar ϕ and has by experiment been shown to be nearly constant.

The k-ε turbulence model is a two-equation model in which two additional transport equations, partial differential equations, are employed to determine the local turbulent viscosity, $\mu(x, y, z, t)$ and so close the conservation equations. Depending on the characteristics of the flow, different transport equations have to be used. Therefore, the k-ε model can be divided into the high Reynolds number and the low Reynolds number k-ε model. [15] In this work the former model has been employed, thus the latter is left without consideration.

The high Reynolds number k-ε model

The Kolmogorov-Prandtl proportionality relates the turbulent viscosity to the kinetic energy k and its dissipation rate ε. Using density-weight averaged quantities:

$$\mu_t = C_\mu \overline{\rho}\frac{\tilde{k}^2}{\tilde{\varepsilon}} \qquad \textit{(Eq. 3.20)}$$

where

ε is the viscous dissipation rate of turbulent kinetic energy, k. The value of ε gives a measure of the irreversible transformation of kinetic energy to heat, thermal energy.

$$\varepsilon = \upsilon_t \overline{\left(\frac{\partial u_i^{"}}{\partial x_j}\right)\left(\frac{\partial u_i^{"}}{\partial x_j}\right)}$$

k as defined by equation 3.18

C_μ is an empirical constant with a value of 0.09. [15]

The turbulence kinetic energy and its dissipation rate are obtained from their transport equations. Mathematically these are written:

Turbulent kinetic energy equation:

$$\frac{\partial}{\partial t}\left(\bar{\rho}\tilde{k}\right)+\tilde{u}_i\frac{\partial}{\partial x_i}\left(\bar{\rho}\tilde{k}\right)=\frac{\partial}{\partial x_i}\left[\left(\frac{\mu_t}{\sigma_k}+\mu\right)\frac{\partial\tilde{k}}{\partial x_i}\right]+\mu_t\left(\frac{\partial\tilde{u}_i}{\partial x_j}+\frac{\partial\tilde{u}_j}{\partial x_i}\right)\frac{\partial\tilde{u}_i}{\partial x_j}-\beta g\frac{\mu_t}{\sigma_t}\frac{\partial\tilde{T}}{\partial x_i}-\bar{\rho}\tilde{\varepsilon}$$

(Eq. 3.21)

where

σ_k is the turbulent Prandlt number for *k*, and

$\beta = -\frac{1}{\bar{\rho}}\frac{\partial\bar{\rho}}{\partial\tilde{T}}$ is a thermal expansion coefficient.

The above equation describes the transport of turbulent kinetic energy through different processes, including convection, diffusion, viscous dissipation et cetera.

Dissipation rate of turbulent kinetic energy:

$$\frac{\partial}{\partial t}\left(\bar{\rho}\tilde{\varepsilon}\right)+\tilde{u}_i\frac{\partial}{\partial x_i}\left(\bar{\rho}\tilde{\varepsilon}\right)=\frac{\partial}{\partial x_i}\left[\left(\frac{\mu_t}{\sigma_\varepsilon}+\mu\right)\frac{\partial\tilde{k}}{\partial x_i}\right]+C_{\varepsilon 1}\frac{\tilde{\varepsilon}}{\tilde{k}}\left(G_K+G_B\right)\left(1+C_{\varepsilon 3}R_f\right)-C_{\varepsilon 2}\bar{\rho}\frac{\tilde{\varepsilon}^2}{\tilde{k}}$$

(Eq. 3.22)

Here

σ_ε is the turbulent Prandtl number for the dissipation of turbulent kinetic energy, ε,

$C_{\varepsilon 1}$, $C_{\varepsilon 2}$ and $C_{\varepsilon 3}$ are empirical constants,

$G_K = \mu_t\left(\frac{\partial\tilde{u}_i}{\partial x_j}+\frac{\partial\tilde{u}_j}{\partial x_i}\right)\frac{\partial\tilde{u}_i}{\partial x_j}$ is a shear stress term,

$G_B = -\beta g\frac{\mu_t}{\sigma_t}\frac{\partial\tilde{T}}{\partial x_j}$ is a buoyancy term, and

$R_f = -\frac{G_B}{G_K}$ is known as the flux Richardson number.

The standard values of the constants in the k and ε equations are those first proposed by Launder and Spalding in 1974, namely

Table 3.1 Constants employed by the standard k-ε turbulence model

C_μ	0.09
$C_{\varepsilon 1}$	1.44
$C_{\varepsilon 2}$	1.92
$C_{\varepsilon 3}$	0.8
σ_k	1.00
σ_ε	1.30

[7, 11, 15, 16]

From the equations for turbulence kinetic energy and its dissipation rate the eddy viscosity, required by the Boussinesq assumption, can be estimated given the proportionalities $\mu_t \sim \rho\, u\, l$ and $u \sim k^{1/2}$, $l \sim k^{3/2} / \varepsilon$.

Several modifications to the standard k-ε model have been proposed. For example Yan and Holmstedt [17] presented a model in which the buoyancy was remodelled. In this work however, the standard model has been adopted for calculations.

3.3. Thermal radiation modelling

The radiation influence has its numerical origin in the energy conservation equation, equations 3.6 and 3.14, where it appears as a source term. In modelling this term, three steps can be distinguished. First, an overall equation to describe radiant transfer, that is, a radiative transfer equation RTE, needs to be established. Second, a way to predict the optical properties for relevant combustion gases and soot particles has to be found. After these initial steps the necessary relationships have been derived and so, a third step will be to find a suitable method to solve the algorithm.

Considering a simple set of control volumes, the most fundamental radiative transfer equation implies that the change in intensity in a certain direction equals the energy emitted from matter within the control volume plus energy scattered into it from the outside minus energy losses by absorption inside the control volume and particle scattering out from it. Mathematically this is expressed using an integrodifferential equation, which in its fundamental form would have to be solved for every wavelength in the spectrum. In the Ω direction the relationship is written as: [16, 18]

$$\frac{dI}{ds} = -(k_a + k_s)I + k_a \frac{E_g}{\pi} + \frac{k_s}{4\pi} \int_{\Omega'=0}^{4\pi} P(\Omega,\Omega')I(\Omega')d\Omega' \qquad \textit{(Eq. 3.23)}$$

I is the radiant intensity in the Ω direction,

s is the relevant distance in the Ω direction,

E_g is the emissive power of gas at the temperature T_g, $E=\varepsilon\sigma T^4$,

$P(\Omega,\Omega')$ is the probability that incident radiation in the direction Ω' will be scattered into the increment of solid angle $d\Omega$ about Ω, and

(k_s+k_a) represents gas absorption and scattering coefficients. Note that under steady state $k_a=\varepsilon$, the so-called Kirchoffs identity, a relationship that can be easily derived using a simple energy balance.

As the radiation time scale is related to the speed of light there is really no need for transient terms.

Thus, in equation 3.23 above:

$-k_aI$ represents radiant loss by absorption

$-k_sI$ represents loss through scattering effects,

$k_a \frac{E_g}{\pi}$ represents gain by emission, and

$\frac{k_s}{4\pi} \int_{\Omega'=0}^{4\pi} P(\Omega,\Omega')I(\Omega')d\Omega'$ represents gain by scattering.

If it is assumed that scattering can be ignored and then integrating, the radiation intensity can be calculated from [19]

$$I_{n+1} = I_n e^{-k_a \Delta s} + \frac{\sigma T^4}{\pi}\left(1 - e^{-k_a \Delta s}\right) \qquad \textit{(Eq. 3.24)}$$

In this case, the radiative transfer equation has been simplified to a recurrence equation in which the intensity on exit, I_{n+1}, is expressed in terms of intensity on entry, I_n.

The second step is related to the fact that the radiation emitted depends on the emissivity and absorptivity which in turn are rather complex functions of a number of parameters such as soot and gas concentrations, temperature, pressure, path length et cetera. The crudest approach to take account of the radiative properties of gases and particles, except from ignoring them, is to give a constant value on the absorptivity coefficient.

Instead of using a constant absorption coefficient, spectral calculations can be performed, in which the thermal electromagnetic spectrum (radiation with wavelengths between 0.1 to 100 μm) is divided into several intervals or bands in order to take account of the variation of the radiative properties with wavelength. The concept is usually divided into groups termed wide-band models or the narrow-band models depending on the characteristics of the intervals. These two approaches have until recently been considered to be slightly too demanding for general use in CFD modelling of fires. However, in reference [18] a fast narrow-band model is presented, also giving a hint of the possibilities of such a model.

Another more crude category of models for the prediction of radiative properties is the so-called “Total absorptivity-emission models”. For given temperatures and pressures the band absorptivities are integrated over the total electromagnetic spectrum. This will result in a number of total absorptivity and emissivity curves. Afterwards, one seeks the appropriate polynomials to fit these curves using regression techniques. In some models, the curve-fitted expressions can be arranged so that the resulting expressions would be presented as the sum of all clear and grey gases. These are so-called weighted-sum-of-grey-gases, WSGG-models. A modified WSGG-model has been used in this work.

Step three in our thermal radiation modelling program is to find a suitable solution procedure for the relationships derived in the previous steps. In the literature, a large number of solution methods are presented and some five families can be distinguished, these are:

- Exact methods
- Statistical methods
- Zonal methods
- Flux methods
- Hybrid methods

As indicated by the name, the hybrid methods can be viewed upon as methods developed by taking advantage of the desirable features of other models. One of these is the discrete transfer radiation model, DTRM in short. Lockwood and Shah [20] first presented this in 1981. Since then, it has become the most commonly used method for solving the integrodifferential radiative transfer equation (equation 3.23 and 3.24) when dealing with fire related problems. The general concept of the discrete transfer method is that it solves the radiation equation along a, user defined, number of discrete rays

from every element of the boundary surface. The directions of these rays are specified in advance and the intensities in between rays are assumed constant. [20]

The radiation energy source term for every computational cell and the net radiation flux to the boundary surface elements are calculated using the intensity obtained from eq 3.23 or 3.24. Again, ignoring scattering the relationships below are used:

$$\dot{q}^R = \oint\oint I d\vec{\Omega} d\vec{A} = \sum_{Rays} \left(I_{n+1} - I_n\right)\vec{\Omega} \cdot \Delta\vec{A}\Delta\vec{\Omega} \qquad \text{(Eq. 3.25)}$$

for the source term, and

$$R_{flux} = \sum_{Rays} I_w \left(\vec{\Omega}\vec{n}\right)\Delta\vec{\Omega} - \varepsilon_w \sigma T^4 \qquad \text{(Eq. 3.26)}$$

for equating net radiative flux.

3.4. Modelling combustion

Combustion is a chain reaction process involving a large sequence of single, elementary reactions, ultimately ending up with a set of products, for hydrocarbons typically carbon monoxide, carbon dioxide and water. Thus the simplest hydrocarbon, methane, burning in air involves over 149 elementary steps, 144 reverse chemical reactions and involving 33 different species. At low temperatures, the steps that are able to initiate the chain reaction are very slow. This is fortunate, because otherwise air and fuel, for example air and wood, could not coexist. [21]

While a rather large scientific community seems to be involved and concerned with general Computational Fluid Dynamics, improvements of turbulence models et cetera, the knowledge in combustion modelling, on the other hand, seems to be restricted to a more less numerous assembly of specialists. One logical reason for this is that combustion science is highly interdisciplinary, requiring knowledge in thermodynamics, chemistry, chemical kinetics and fluid mechanics. In this work the eddy break-up model presented below has been used to model the combustion process.

3.4.1 Eddy Break-up/Magnussen dissipation concept

The Eddy Break up model has experienced a world-wide spread and acceptance. It originates from Brian Spalding's (1971) [22] model for premixed flames and have since been modified to some extent for use with diffusion flames [9]. In the Eddy break up model, all the detailed chemical kinetics have been dropped. Instead, combustion is assumed to be infinitely fast and to follow a single one-step stoichiometric chemical reaction, for a general case written as

1 kg fuel + s kg of oxidant $\rightarrow$ *(1+s) kg of products* *(Eq. 3.27)*

where *s* represents the stoichiometric fuel to oxidant ratio and the *products* are carbon dioxide and water. Note that the general reaction above is written using the masses of fuel, oxidant and product species and not their volumes.

As the chemistry process is assumed to be infinitely fast the reaction rate will be controlled by mass transfer, primarily by the turbulent mixing of reactants which in turn

is dependent on the breaking up of eddies in the turbulent flow field. Three subprocesses will then control the reaction rate; these are the turbulent dissipation of fuel, oxidant and products. The model takes the local reaction rate, that is the rate at which the fuel is consumed at a certain location, to be the slowest of the three mixing processes referred to above. Mathematically this is expressed as

$$R_{fu} = -\bar{\rho}\frac{\varepsilon}{k}\min\left[C_R\bar{Y}_{fu}, C_R\frac{\bar{Y}_{ox}}{s}, C'_R\frac{\bar{Y}_{pr}}{1+s}\right] \qquad \textit{(Eq. 3.28)}$$

where

R_{fu} is the mass rate of fuel consumption, rate of reaction,

$\frac{\varepsilon}{k}$ is the turbulence time scale,

C_R, C'_R are empirically derived factors often expressed by constant values, or some simple relationship including turbulent kinetic energy, k, and its dissipation rate, ε, as variables.

$\bar{Y}_{fu}$, $\bar{Y}_{ox}$, $\bar{Y}_{pr}$ are the time averaged mass fractions of fuel, oxidant and hot products respectively.

The model can be made more sophisticated in many ways for example by incorporating soot models and models for NO_x concentration [9]. In addition, equation 3.28 can be extended to include the influence of chemical kinetics.

Using the Arrhenius expression for the rate of reaction [13],

$$R_{fu} = A\rho^{-a}Y_{fu}{}^{b}Y_{ox}{}^{c}\exp(-E_a/RT) \qquad \textit{(Eq.. 3.29)}$$

Equation 3.28 then becomes

$$R_{fu} = -\min\left[\bar{\rho}\frac{\varepsilon}{k}C_R\bar{Y}_{fu}, \bar{\rho}\frac{\varepsilon}{k}C_R\frac{\bar{Y}_{ox}}{s}, \bar{\rho}\frac{\varepsilon}{k}C'_R\frac{\bar{Y}_{pr}}{1+s}, -R_{fu,kinetic}\right] \qquad \textit{(Eq. 3.30)}$$

By adopting equation 3.28, the task of the combustion model has been reduced to the solution of the species concentration equations for fuel, oxidant and products. At this point, it is convenient to introduce the mixture fraction, *f*, which is a dimensionless number defined as

$$f = \frac{\beta - \beta_{ox}}{\beta_{fu} - \beta_{ox}} \qquad \textit{(Eq. 3.31)}$$

where

$$\beta = sY_{fu} - Y_{ox}$$

The subscripts *fu* and *ox* denotes fuel and oxidant streams respectively.

This operation is mathematically convenient because now only the fuel mass fraction and a transport equation for the mixture fraction need to be solved. The oxygen and product concentrations are then given from Equation 3.27 and the chemical species conservation. [19]

The model has proved to give reasonably good predictions, however its reliability depends on a number of factors, most important the performance of the turbulence model.

3.4.2 Flamelet model

The flamelet model is probably the most interesting near-future combustion model. Here a turbulent flame is considered to consist of a large number of small laminar flames, called flamelets. Statistical information concerning the mixture fraction fluctuation is stored in a probability density function, PDF, usually in the form of a beta function. From the first and second moment of this PDF, that is the Favre averaged mixture fraction and its variance, the turbulent mixing of scalars can be described.

This method have the main advantage that it brings the simulation closer to the true nature of combustion and thus allows for more proper account of for example chemical species and soot.

3.5 Summary

To sum up, the basic physics of fluid flow and combustion modelling has been addressed as being a somewhat fundamental part of the project. The theory has been limited to involve the basic modelling approaches used in the present work including conservation equations, the effect of turbulence, thermal radiation and some basic comments on the modelling of combustion.

By introducing different kinds of subgrid models instead of solving the governing equations directly the CFD, or field model, ceases to represent an exact science. Considering the available computer power, present and in the near future, approximations and empirical relationships are essential in order to proceed. For example, using one of the modern “super computers” it is actually impossible to make direct simulations of flows given a moderately high Reynolds number.

4. Flaming ignition and flame spread on a solid surface

Ignition of a solid fuel can occur either within the solid or in the gas phase, where the latter is referred to as flaming ignition. The subsequent combustion process can take place within the subsurface layers of the solid (smouldering combustion), at the solid-gas interface (glowing combustion) or in the gas phase (flaming combustion).

When ignition takes place without the presence of a pilot source, such as a small flame or an electric spark, it is referred to as spontaneous- or auto-ignition. If a pilot source is present, locally inducing a combustion reaction, which then are free to propagate, causing flame spread, the phenomena is called piloted ignition.

Piloted ignition can be achieved with a certain, material dependent, minimum required heating or incident heat flux, at and below which the flame would not sustain itself if the external heating was to be removed. This is sometimes referred to as transient ignition. To make the combustion process self-sustained after the external heating is removed, referred to as persistent ignition, a larger amount of energy is required.

This work is mainly interested in the piloted, gas phase ignition phenomena and the purpose here is merely to point out some of the difficulties in dealing with ignition and flame spread.

4.1 Theoretical description of ignition

Kanury [23] differs between three coarsely grouped factors that govern the actual time to ignition of a solid fuel. These are:

1. The degradative thermal response of the solid to yield combustible gases, including the heating and gasification of the solid fuel,
2. The boundary layer mixing of the combustible gases with an oxidant (the oxygen in air in most cases), and
3. The induction of the temperature- and composition-dependent rate of the combustion reaction to a sufficiently high level to be self-supporting, including the onset of gas phase chemical reaction.

Clearly, for piloted ignition, in which some pilot source is applied to initiate a combustion reaction in the boundary mixture, the first and second factors would suffice to reach continuos self-sustained reaction. If the solid is to ignite without the presence of a pilot its temperature, the rate of pyrolysis etc has to be relatively high.

It is intuitively recognised that various materials have different “ignition inertia”, i.e. the time to ignition at a certain exposure can differ a great deal. Figure 4.1 illustrates the auto-ignition delay times as function of the initial surface heat flux and the velocity of an ambient (hot) gasflow, in figure 4.1 represented by the stretch rate “a”. The figure originates from the experiments on spontaneous ignition of solid polymers in high temperature oxidising flow, of Niioka [24]. Note that the velocity of the flow is expressed in terms of the stretch rate, a, and that the stretch rate increases as the convective velocity increases.

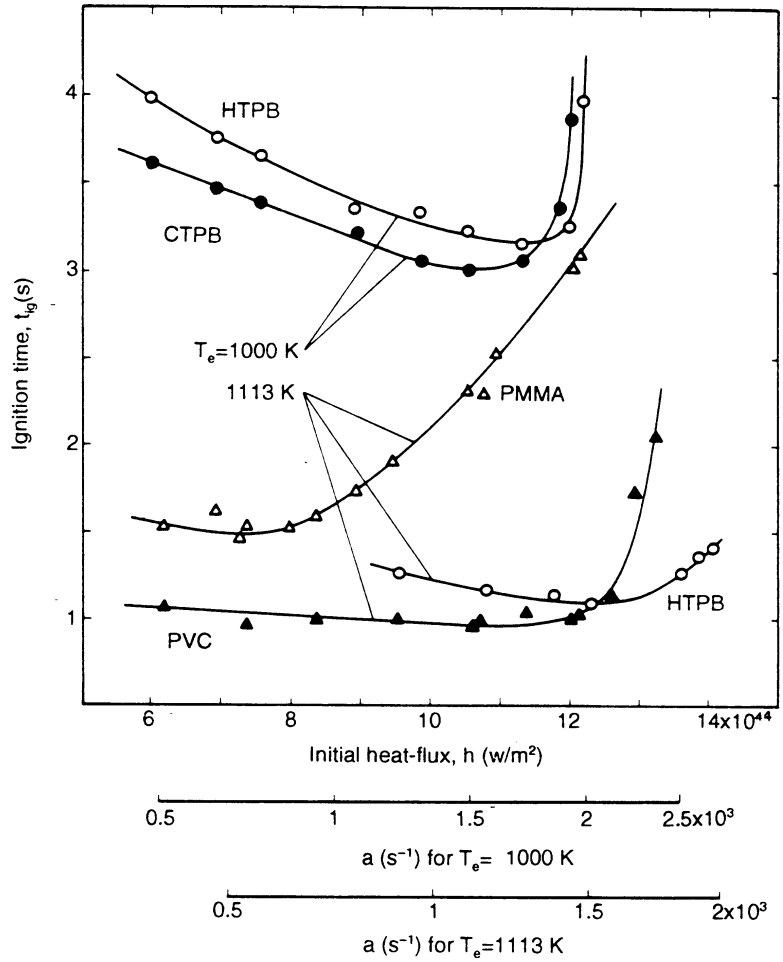

Figure 4.1 Ignition time as function of initial heat flux and stretch rate at two different temperatures. From [25]

It can be observed that as the flow velocity is increased the ignition time first decreases then after reaching a minimum value increases. These results imply that the ignition process is controlled by different mechanisms and that these mechanisms exert influence at different exposure conditions. By considering the factors named above this can be easily interpreted. If the flow velocity is increased (increased stretch rate) the surface heat flux will increase and as a result the time to ignition will decrease. Thus the initial slope is likely to be attributed to the thermal response of additional heat flux, factor number 1 above. If, on the other hand the gas phase factors are considered (number 2 and 3), an increase in flow velocity will result in a decrease in the flow residential time which, if comparable with the chemical time, will delay the onset of a chemical reaction, and ultimately prevent its initiation.

The concept can be summarised using two different time scales, the pyrolysis time describing the influence of the thermal response of fuel and induction time representing gas phase mixing and reaction factors as illustrated in figure 4.2. A small induction time will thus imply a low velocity flow with high oxygen concentration and high gas temperatures, or piloted ignition.

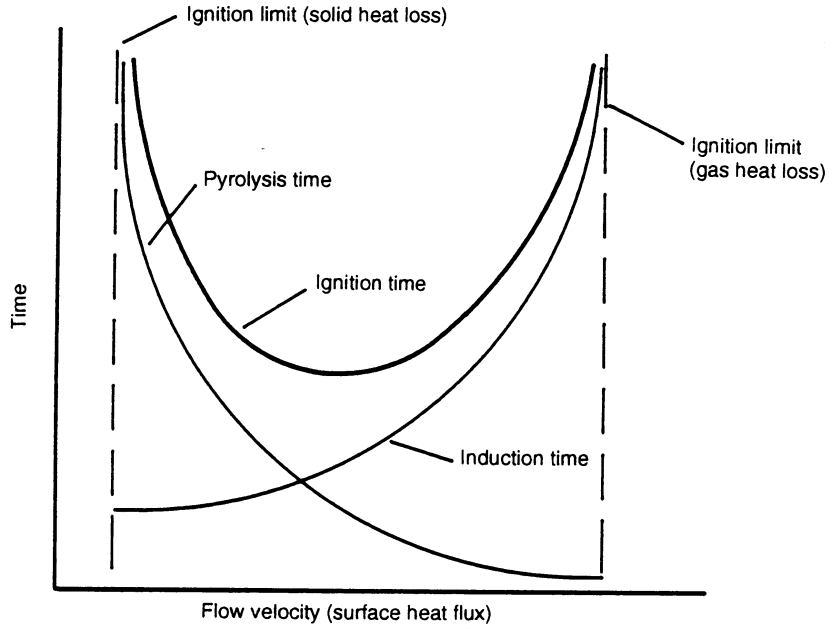

Figure 4.2 Qualitative illustration of ignition mechanisms and ignition time variations. [25]

For a vertical plate it is clear that, due to the thickening of the boundary layer, both surface heat flux and the ratio of the flow residential time to the chemical time decrease with the distance from the leading edge. Ignition delay time and the location of ignition will be governed by the characteristics of the flow so that for long gas induction times ignition will be delayed and its initiation will be downstream of the leading edge of the plate. Consequently, if the gas induction time is short, for example if convection from buoyant hot gas is a dominant mode of heat transfer, ignition will be controlled by heat transfer to the solid plate and occur near the leading edge. Introducing a pilot flame will result in locally reduced induction time. So, the heating of the solid will be the dominant factor unless flow is very fast or oxygen concentration very low.

Considering a schematic picture of the different component processes, figure 4.3, the complexity of the problem can be imagined. The incident heat flux, i [kW/m^2], is partly conducted into the solid fuel, partly reradiated to the surroundings and partly dispersed by natural convection, all three of these transport processes are highly transient.

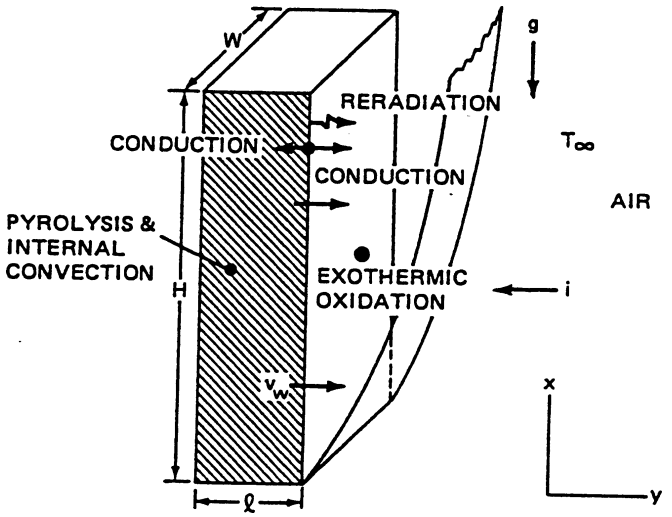

Figure 4.3 Schematics on heat transfer mechanisms. [23]

As the layer heated by conduction reaches 100°C free moisture will be evaporated and flow, primarily, out from the solid. A small part of the vapour will move into the cold, virgin, fuel, subsequently causing a heat sink and also modifying the original solid physically and chemically. Conditions for pyrolysis is first reached in a layer close to the surface and as heat is continuously conducted into the fuel the pyrolysis front moves towards deeper layers forming a porous carbonaceous char. The pyrolysis gases flow outwards through the char inducing an internal convective flow thus counteracting with the conductive heating.

If the pyrolysis gases entering the gas phase boundary layer are non-combustible the temperature profile will be continuously decreasing as function of the distance from the solid surface into the gas. However, if the pyrolysates are combustible the temperature profile will reach a maximum somewhere in the gas phase boundary layer due to oxidative energy release. The temperature responds to the reaction rate that is assumed to be zero at the boundary edge and maximum inside the gas-layer. As these oxidative processes evolve heat transfer from solid to gas will decrease and ultimately the temperature gradient at the solid surface will change sign. This will be one of the possible criteria for characterising flaming ignition, which is addressed below.

Theoretical criteria for (flaming) ignition

To be able to theoretically predict the inception of ignition an ignition criteria have to be identified and quantified. When modelling ignition and the following flame spread and fire growth it is desirable to restrict the criterion and preferably choose only one. The critical values for ignition are in general derived experimentally. Kanury [23] summarised some existing criteria, proposed by various investigators, as follows.

- ✓ $T_{s,\text{interface}} \geq T_{ig1}$ — Critical temperature in gas phase-solid interface
- ✓ $\overline{T_s} \geq T_{ig2}$ — Critical average solid temperature
- ✓ $\dot{m}''_{\text{interface}} \geq \dot{m}''_{\text{crit}}$ — Critical pyrolysate mass flux (usually in the range 10^{-5}-10^{-4} g/cm^{2}s)
- ✓ $\delta_{\text{char}} \geq \delta_{\text{crit}}$ — Critical char depth
- ✓ $\frac{\partial T_g}{\partial t} \geq R_{1,\text{crit}}$ — Critical increase rate of local gas temperature
- ✓ $\int (\textit{reaction rate}) dy \geq R_{2,\text{crit}}$ — Critical total reaction rate in the boundary layer
- ✓ $\left(\frac{\partial T_g}{\partial y} \right)_{\hat{y}=0} = 0$ — Gas temperature gradient reversal at the gas phase-solid interface

Another rather fundamental ignition criteria, not mentioned specifically by Kanury, would be to consider the total absorbed energy in the solid and to identify some “critical” accumulated energy value.

- ✓ $\int \dot{q} dt \geq R_{3,\text{crit}}$ — Critical accumulated energy in the solid

4.2 Flame spread

Flame spread on solid fuels is a very complicated process in which a number of interacting physical and chemical processes are involved, both in the solid and the gas phase. The processes are usually transient and exhibit non-linear features.

The governing mechanisms and their influence of flame spread are somewhat different depending on what direction of spread is considered. In this work only the upward concurrent flow flame spread that is the spread in the direction of the ambient (buoyancy driven) flow, is considered. For this case a simple description of thermal influence of the fuel can be illustrated as in figure 4.4, where the arrows indicate incoming heat flux and flow of pyrolysis gases.

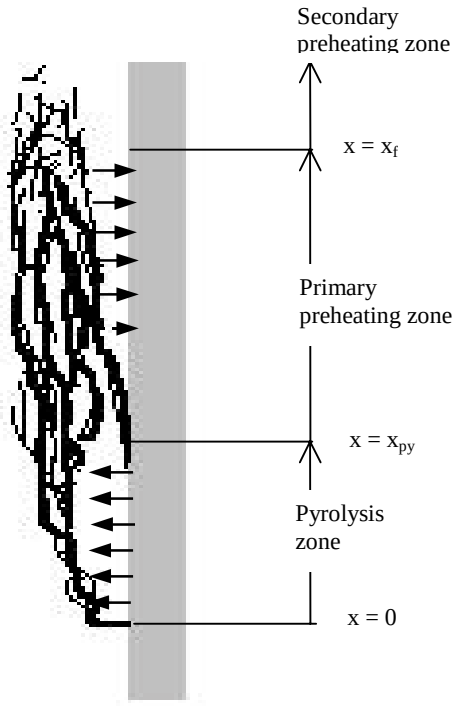

Figure 4.4 Illustration of concurrent upward flame spread. Note that the x-scale is moving upward as flame spread continues and fuel becomes burnt out.

Experimental results from upward turbulent flame spread, with moderately large fires having a flame height less than 1.4 meters, indicates that the heat flux ahead of the pyrolysis zone is almost independent of material characteristics and can, for free upward flame spread, be approximated to 25 kW/m^2. However it has also been shown that both laminar and large fires can exceed this heat flux. [26]

Through phenomenological arguments and non-dimensional flat plate boundary layer analysis it has been concluded [25] that the controlling mechanism for concurrent flow flame spread is related to the heat transfer from the flame to the solid fuel ahead of the pyrolysis front. The chemical kinetics in the gas phase was determined to have influence on the rate of flame spread though the characteristics of the flame such as flame length, temperature and the presence of soot.

4.3 Flame spread modelling

In the last decade several groups of scientists, working separately in various countries, have developed flame spread theories that can be used in an engineering fashion to calculate flame spread and the resulting fire growth. These methods are of various degrees of sophistication and complexity. Some give approximate answers for specified end-use scenarios, can be used by non-experts and require simple input. Others are more general and more flexible, but may require expert knowledge and large amount of input data.

From the earlier discussion it is evident that one of the most crucial parts in flame spread modelling is to accurately predict the heat transfer, and particularly the radiative part, to the virgin solid. The two physical processes are directly linked to each other through for example soot concentration and local gas temperature.

Mainly two types of methods for such predictions, in practical end-use scenarios, have been proposed in the literature. Firstly, purely thermal models for upward flame spread have been used, with input data from the Cone Calorimeter, to predict flame spread in large scale and the resulting heat release rate. Secondly, more fundamental work has been carried out using CFD models and pyrolysis models to predict fire growth.

4.3.1 Thermal theory models

It has been experimentally shown that flame spread over solid continuos surfaces can be treated as the movement of an ignition front characterised by the ignition temperature of the solid fuel. In this treatment the chemical and physical features of pyrolysis and gas phase mixing is omitted from analysis and the fuel can be treated as being inert. Purely thermal theories can then be used to calculate surface temperatures on a solid and as soon as an element reaches the ignition temperature, that element is assumed to pyrolyse. Often, the element is then assumed to release a certain, predetermined, amount of energy usually linked to heat release rate measurements from the Cone Calorimeter. Such an approximation eliminates the need for calculating the mass flow rate of combustion gases from the solid element and consequently, no account of chemical kinetics has to be taken.

Very many different approaches to such modelling have been made where the results have been compared to experiments involving practical building materials. All of these require that the flame morphology, specifically the flame length, be estimated as well as the heat flux from the flame to the solid materials. It is generally difficult to estimate these variables and many workers have therefore opted for making relatively simple assumptions with respect to flame lengths and flame heat fluxes.

Hasemi [27] used a variable flame heat flux to analyse temperature rise of the unburned fuel ahead of the pyrolysis front. Delichatsios [28] and Beyler [29] also used expressions for a variable heat flux over the flame height to calculate the upward flame spread velocity and fire growth.

One of the most straightforward approaches is characterised by assuming a simple relationship between flame length and heat release rate and assuming a constant flame heat flux over this length, as Saito et al. [30] did. This led to an analytical model for upward flame spread velocity V(t) involving a Volterra-type integral as shown below Eq 4.1.

$$V(t) = \frac{y_{flame} - y_{py}}{\tau}$$

$$V(t) = \frac{1}{\tau}\left[\underbrace{K\left(\dot{Q}_b + y_{py,0} W\dot{Q}''(t) + \int_0^t W\dot{Q}''(t - t_p)V(t_p)dt_p \right)^n}_{flamehight} - \underbrace{\left(y_{py,0} + \int_0^t V(t_p)dt_p \right)}_{height\ of\ pyrolysis\ front} \right]$$

(Eq. 4.1)

Here, the terms in the bracket represent flame height and height of pyrolysis zone respectively and τ is the time to ignition.

Thomas et al. [31] solved the Volterra equation and Karlsson [32] used this approach to develop a model for predicting flame spread and fire growth in several geometries, including the Room Corner test. This model requires that the material be tested in the Cone Calorimeter at a number of different heat flux levels in order to derive an apparent thermal inertia, $k\rho c$, which is used to calculate time to ignition. The heat release rate data from the Cone Calorimeter, and the $k\rho c$ value, is then used to calculate flame-spread velocity and heat release rate in the large-scale test (for example the Room Corner test).

Several models of this type have been described in the literature, only a few are mentioned here as examples. Cleary and Quintiere [33] developed a method that allowed both upward and lateral flame spread to be calculated, using data from the Cone Calorimeter and the LIFT apparatus. Baroudi and Kokkala [34] developed a computer program to solve the Volterra-type integral equation and Kokkala et al. [35] tested it against experiments, using Cone Calorimeter data as input.

Many of the applications have only compared the calculated results with a very limited number of full-scale experiments, but Karlsson [36] used 22 different Room Corner test experiments and compared calculated and experimentally measured heat release rates. The experimental data originates from two series of experiments, the S-series [37] and the E-series [38]. Figure 4.5 shows the heat release rate history of four of these materials, showing good agreement with experimental measurements.

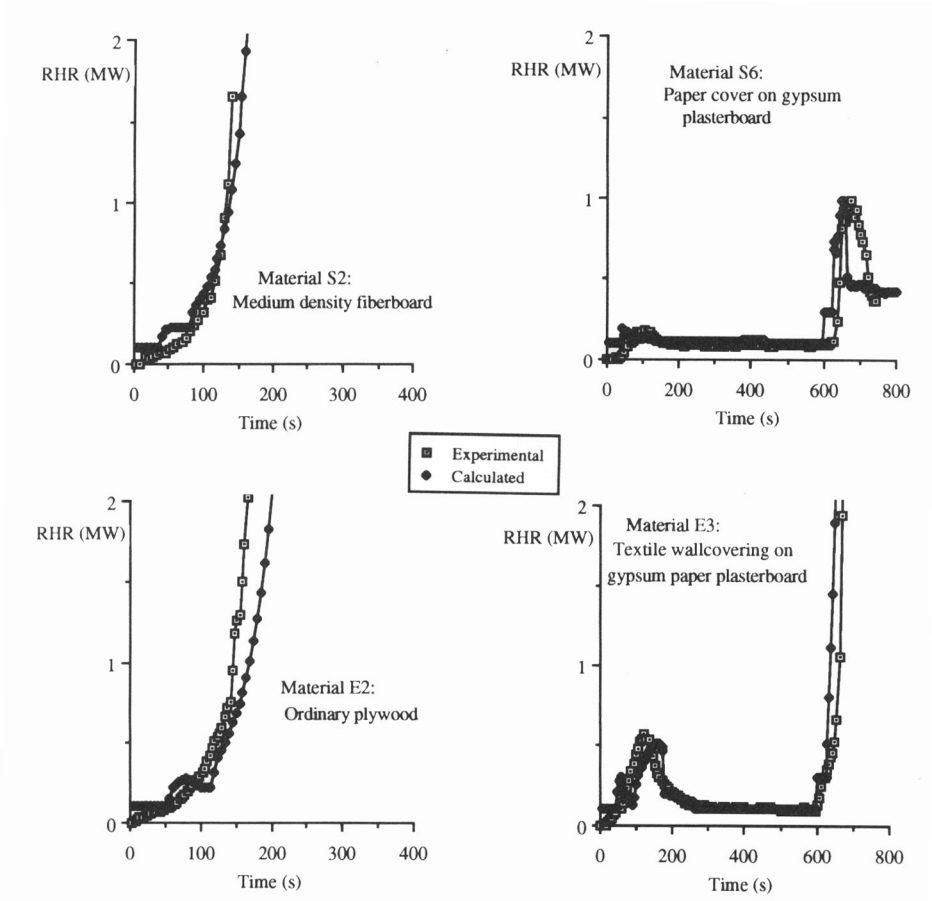

Figure 4.5 Comparison of calculated and measured heat release rates from the Room Corner test for 4 different surface lining materials (from [36]).

Figure 4.6 shows calculated and experimentally measured time to flashover for all 22 materials tested. Only 2 out of 22 materials deviate significantly. Some of the materials did not go to flashover in the Room Corner test, this is indicated by the longest bars in Figure 4.6.

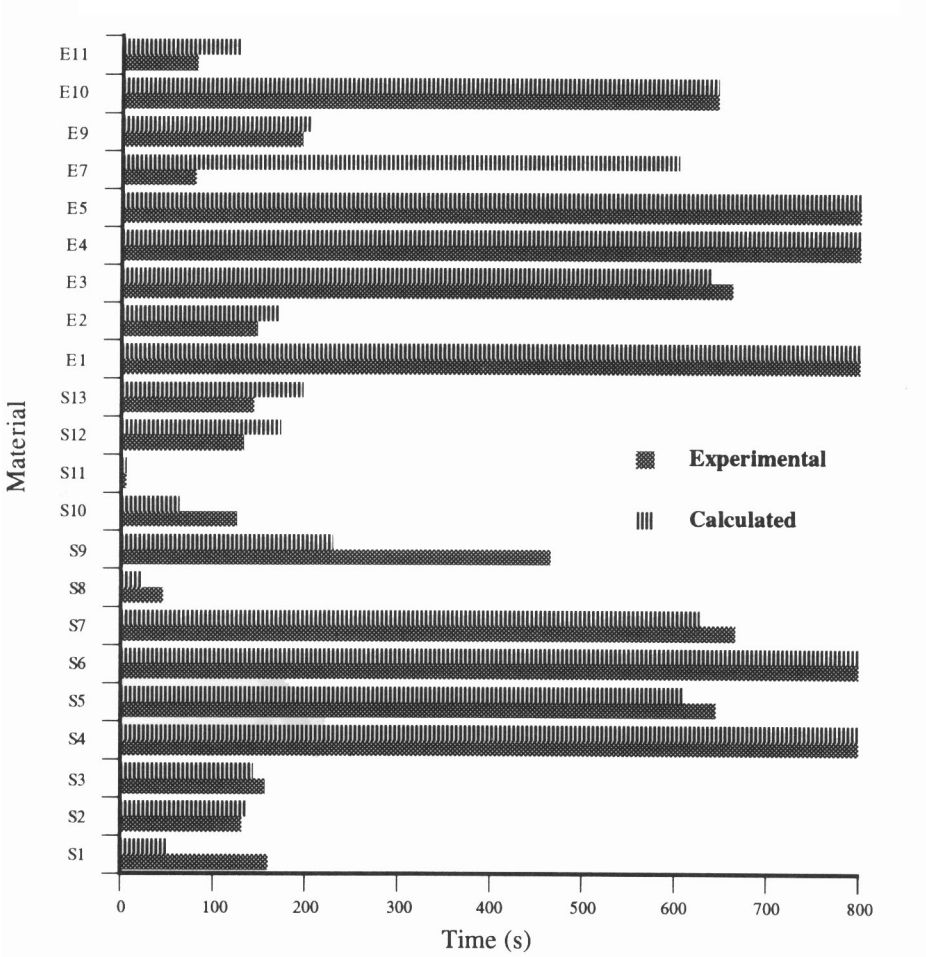

Figure 4.6 Calculated and experimental time to flashover in the Room Corner test for 22 different surface lining materials (no flashover after 800 s). From [36].

Many other models than those mentioned above have been used for predicting full-scale fire growth using input data from the Cone Calorimeter. This section has concentrated on upward flame spread on practical surface lining materials, and results have only been shown displaying their behaviour in the Room Corner test.

Despite the qualitatively sound predictions made by these kinds of models it should be recognised that the underlying theory is to a high degree built upon rather ambiguous assumptions and approximations. The fundamental hypothesis in equation 4.1 is that the flame spread can be described by a time to ignition at a given, normally prescribed, heat flux, and the difference between a flame height and a pyrolysis height where both the height of flame and that of the pyrolysisfront are assumed to be constant. Furthermore, the incident heat flux from the flame is given a constant value, derived from small-scale experiments, and no secondary pre-heating above the flame is assumed to take place. Yet, the height of flame is generally not constant nor is the incident flux. Figure 4.7 gives an illustration of the variation in flame height for a burner with a total rate of heat release 300 kW. At smaller rate of heat release the intermittence would be even larger. These fundamental discrepancies indicate that the thermal model may need to be reconsidered even in its most fundamental parts and consequently more physically sound approaches relating solid flame spread phenomena to the laws of mass and energy transfer within the materials are developed. These new models use different kinds of pyrolysis models and incorporated into a robust CFD code, solving equations for turbulent reacting flow; most of the crude assumptions used by the thermal models can be excluded. Also, as these models are initially derived from first principles their applicability can be assessed qualitatively from the underlying physics.

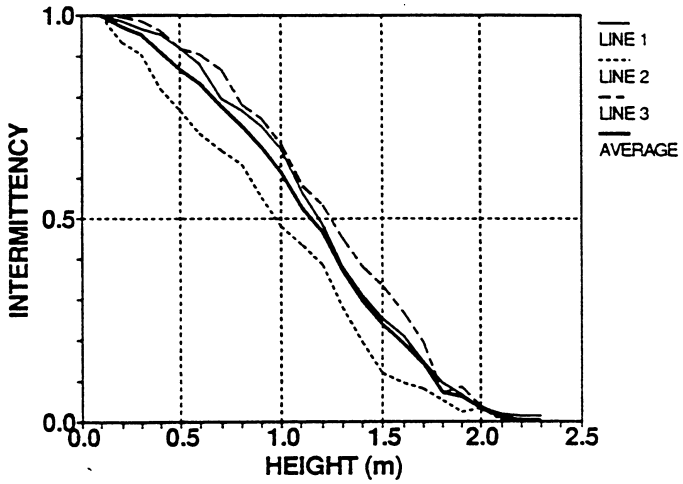

Figure 4.7. Flame height intermittence as function of vertical distance from the surface of the burner at a heat release rate of 300 kW. The different lines denote different locations relative to the centreline. [39]

4.3.2 Physical flame spread models using pyrolysis models

Since CFD models allow variables to be calculated locally in a very fine mesh, there is no need to make any rough assumptions on flame height and heat flux made by the thermal models. This open up possibilities for more sophisticated models, both for calculating solid material temperatures, mass flow rate of pyrolysis products from the solid material and the subsequent combustion of these pyrolysates. However, for some applications, data from the Cone Calorimeter can be used instead of calculating the pyrolysis and the combustion process.

Even though this approach is more flexible and easily deal with more fundamental physics, a number of simplifications are needed depending on the requested complexity of the model. For example, heat transfer is often taken to be one-dimensional, the backface of the solid as well as its edges are normally assumed impervious to both heat and mass transfer. The properties of the virgin solid and the carbonaceous residual (char) are sometimes set equal or assumed different but constant in time and space and the pyrolysis gases are assumed to flow through the char without any resistance. Also, the chemical kinetics of pyrolysis, if accounted for at all, is taken to follow a single step Arrhenius rate law with an order of unity. It can be argued that the Arrhenius physics may be ignored for most combustible solids, as the nature of pyrolysis is endothermic and the activation energy so high that the reaction essentially becomes determined by heat transfer in and through the solid.

If the pyrolysis model is incorporated into a CFD code no further assumptions are required for the gas phase effects as necessary properties are provided from the modelling of turbulent combustion.

As an example of this approach, Yan and Holmstedt [40, 41, 42] presented a general pyrolysis model embedded in a CFD code for predicting flame spread on a vertical PMMA slab (non-charring) and on particle board (charring material). Both the turbulent combustion of the gas phase and the pyrolysis of the solid fuel were numerically simulated. The pyrolysis model makes it possible to more properly account for the effect of heat flux on the resulting rate of heat release. Tuovinen et al. [43] have

implemented this model into the CFD code SOFIE [44] and tested it for other types of materials, showing good results.

The model is based on a one-dimensional numerical heat transfer model that uses a standard numerical solver for the heat conduction equation. Heat conduction in the solid (the wall) parallel to the face of the solid is ignored. Each numerical heat conduction strip is then divided into a number of small elements (stripes) according to the gas phase grid, to which a simple pyrolysis model is applied.

The conservation equations essential for describing the solid phase are the mass continuity and energy equations. The momentum equation is made nonessential by the assumption that the pyrolysates flows through the char with no resistance. By assuming no secondary reaction in the charred area and reducing the three-dimensional problem into one dimension, thus focusing on the dominant perpendicular direction of mass and heat transfer we have:

$$\frac{\partial}{\partial t}\left(\rho_{vir}+\rho_{char}\right)+\frac{\partial \dot{m}''_{vol}}{\partial x}=0 \qquad \textit{(Eq. 4.2)}$$

$$\frac{\partial\left(\rho_{vir}h_{vir}+\rho_{char}h_{char}\right)}{\partial t}+\frac{\partial\left(\dot{m}''_{vol}h_{vol}\right)}{\partial x}=\frac{\partial}{\partial x}\left(k\frac{\partial T}{\partial x}\right)+\dot{q}'''_{py} \qquad \textit{(Eq. 4.3)}$$

In words equation 4.2 states that the instantaneous rate of pyrolysis equals the local gradient in mass-flow of pyrolysis gases. The terms in the energy equation are energy accumulation rate in the solid (energy "storage"), internal convection from pyrolysate flux, conduction and the fourth term represent a pyrolysis sink.

By combining equations 4.2 and 4.3, and applying a few simplifying assumptions, the heat conduction equation on which the model is based becomes [40],

$$\frac{\partial\left(\rho H\right)}{\partial t}+\dot{m}'''\left(H_{py}+H\right)+\frac{\partial\left[\dot{m}''\left(H_{vol,T}-H_{vol,T_{py}}\right)\right]}{\partial x}=\frac{\partial}{\partial x}\left(k\frac{\partial T}{\partial x}\right) \qquad \textit{(Eq. 4.4)}$$

where the variables without subscripts represent solid parameters and

$\dot{m}''' = -\frac{\partial \rho}{\partial t} = \frac{\partial \dot{m}''}{\partial x} \geq 0$ is the mass loss rate per unit volume,

$H_{py} \equiv H^{*}_{vol,T_{py}} - H^{*}_{s,T_{py}} = H^{*}_{vol,T_{py}} - \left(H^{*}_{s,T_0} + \int_{T_0}^{T_{py}} c_p dT \right)$ is a definition of the (material dependent) heat of reaction of the pyrolysis process. Its value is here taken as constant through pyrolysis and this definition is interpreted as the difference in total enthalpy (indicated by the star-superscript) between volatile pyrolysates and the virgin solid at pyrolysis temperature. The integral in the brackets on the RHS is the energy required for preheating.

$H = \int c_p dT$ is the enthalpy of the solid.

$\frac{\partial\left[\dot{m}''\left(H_{vol,T}-H_{vol,T_{py}}\right)\right]}{\partial x}$ represent the heat needed to heat the pyrolysis gases as these flow towards the solid surface. This term is not required for non-charring materials, such as PMMA and usually it is omitted from the subsequent calculations hence the pyrolysis gases are assumed to reach the solid surface directly and with no resistance or heating.

For non-charring materials equation 4.4 can be rewritten, assuming no heat or mass transfer through the back face of the solid:

$$\rho c_p \frac{\partial(T)}{\partial t} + \dot{m}''' H_{py} = \frac{\partial}{\partial x}\left(k \frac{\partial T}{\partial x}\right) \qquad \textit{(Eq. 4.5)}$$

The subsequent assumption is that the material will be pyrolysing only when its temperature has reached the pyrolysis temperature and that temperature gradient in the material will be small (mathematically = 0) thereafter. Thus, the temperature will be constant throughout the whole pyrolysing process, adjusted by the endothermic pyrolysis reaction, until the point where all fuel has been consumed and we can rewrite: [40]

$$\rho c_p \frac{\partial(T)}{\partial t} = \frac{\partial}{\partial x}\left(k \frac{\partial T}{\partial x}\right) \text{ for } T \le T_{py} \text{ and/or } \rho \equiv \rho_{char} \qquad \textit{(Eq. 4.6)}$$

$$\dot{m}''' H_{py} = \frac{\partial}{\partial x}\left(k \frac{\partial T}{\partial x}\right) \text{ for } T \ge T_{py} \text{ and } \rho > \rho_{char} \qquad \textit{(Eq. 4.7)}$$

The following mathematical treatment, discretisation and numerical solution are rather straightforward and are not discussed in this report.

The input parameters used in the pyrolysis model are:

- Pyrolysis Temperature (K)
- Heat of Pyrolysis (J/kg)
- Heat of Combustion (J/kg)
- Virgin Density (kg/m^3)
- Char Density (kg/m^3)
- Specific Heat (J/kg K)
- Thermal Conductivity (W/mK)

An even simpler approach to incorporate flame spread into a CFD code was recently presented by Rubini and co-workers [45]. They developed their model with the intention of reducing the number of detailed solid phase input variables to a minimum. In doing this the input will be of more empirical character, using readily measurable, parameters and less based on first principles. Thus, the model employed disregards the detailed physics of pyrolysis, such as internal heat conduction and char depth.

The flame spread model accounts for preheating and a subsequent transient pyrolysis. Ignition of the virgin solid is assumed related to a certain critical accumulated energy, $E_{critical}$, expressed in terms of incident heat flux through time:

$$E_{critical} = \int_0^{t_{ignition}} \dot{q} dt = \sum_0^{t_{ignition}} \max\left(\dot{q}_{total} - \dot{q}_{\min}, 0.0\right)\Delta t \qquad \textit{(Eq. 4.8)}$$

where q_{total} represent the total, radiative and convective, incident heat flux to the solid surface and q_{min} is a critical incident heat flux below which no ignition can occur.

Once the critical energy has been reached the solid fuel is assumed to release pyrolysis gases at a rate determined by the total incident heat flux and the heat of gasification.

$$\frac{dm}{dt} = \frac{\dot{q}_{net}}{H_g} \Delta A_{face} \qquad \textit{(Eq. 4.9)}$$

where H_g is the heat of gasification and ΔA_{face} is the face area of the computational cell under consideration.

For charring materials the change in rate of pyrolysis, caused by the formation of the char layer, can be accounted for by defining the heat of gasification as function of accumulated mass loss of the solid fuel or by introducing an additional parameter into equation 4.9 simply relating the mass flux to the char-depth.

Many simple flame spread models use the heat of gasification as input variable. Independently of their similar definitions the heat of gasification and the heat of pyrolysis should not generally be confused. For thermally thick vaporising materials at steady state the local heat of gasification H_g is determined from the definition:

$$H_g \equiv \frac{\dot{q}_{net}}{\dot{m}_{total}} = \frac{h_c\left(T_{surr} - T_{x=0}\right) + R_{flux}}{\dot{m}_{total}} = H^*_{vol,T_p} - H^*_{s,T_0} = H_{py} + \int_{T_0}^{T_p} c_p dT$$

This is not a material property and normally it is not constant through the pyrolysis process even though a constant value can be motivated for thermally thick materials [46].

5. The field model SOFIE

The simulations in this work have been carried out using the field model SOFIE, Simulation Of Fire In Enclosures. SOFIE has been developed under the umbrella of a consortium including several European fire research laboratories and Universities. The main participants are: Cranfield University where the SOFIE project was initiated, Lund University, Fire Research Station, Swedish National Testing and Research Institute, Technical Research Centre of Finland, CSTB (France), Home Office Fire Safety Engineering Group, Health & Safety Laboratory.

The principal objectives in developing this CFD code are defined as:

- To develop a field model specifically for the prediction of fires in buildings, that incorporates the core features of current commercially available, general-purpose fluid dynamic computer codes.
- To develop within the code a range of fire specific features to enable prediction of more complex fire phenomena not normally accessible in general purpose codes. For example, fire growth and spread, toxic emissions and dispersion, fire and water spray interaction.
- To make available to the fire science community a robust field model that may be used for both fire safety assessment and as a well-validated common benchmark for comparison with other codes. [47]

Until today, the main work has been towards the development and incorporation of new and more sophisticated models. The latest version of the code used in this work was distributed in May 2000.

5.1 The pre-processor

SOFIE uses a text interface pre-processor. There are two approaches in setting up a problem: to follow the text menus systematically or to write a text file in which all commands are written in the proper order. In reality the text file method is the only practical way, however, this implies that all relevant commands and the order in which these are to be given to SOFIE have to be known by the user.

In the new versions of the code the computational grid is most conveniently created using some CAD-application in which the geometry and the computational domain is constructed. The input of such a drawing to SOFIE must be in VRML1 (Virtual Reality Modelling Language) format.

5.2 Solver

The simulation can be run in steady state or in (first order implicit) transient mode. Using the steady state mode the solution obtained will represent the appearance after what is effectively an infinite amount of time. When running a transient simulation the number of calculation steps per unit time are set by the user. The transient solution approach will of course use much more CPU time then will the steady state, but indeed, the use of steady state simulation may sometimes be questionable.

The base code includes several different optional solvers such as Line by line Gauss-Seidal, Bi-linear-, ILC-, IC pre-conditioned conjugate gradient solver (biccg, iluccg, iccg) and Stones strongly implicit procedure (sip3d).

The interpolation schemes available for relating the nodal value of the dependent variable to the cell face include upwind, hybrid, powerlaw, TVD, QUICK, UQUICK, SOUP and central. [14]

5.3 Output and post-processor possibilities

The present version of SOFIE uses a simple text interface. Results from simulations can be printed in text form on the screen or be exported in different data formats to be viewed using other computer software. An easily available approach is to export a variable profile as a text file and use for example Excel-spreadsheet or similar to prepare the results. Another approach is to make use of some of the commercially available CFD visualisation packages. SOFIE is at present capable to export data in either plot3d, a format that is recognised by most available visualisation software, or fieldview format, a separate format for use in the commercially available Fieldview software package. Using these programs to present results from a simulation in a colourful manner has become an art performed by the members of the CFD community. However, it is an unfortunate fact that this procedure is somewhat time consuming.

6. Using CFD in modelling fire exposed facades

One of the main objectives in this work has been to investigate the use of the CFD code SOFIE, presented in chapter 5, for predicting thermal exposure of a facade given a post-flashover fire in a compartment. Also, a scenario where an outer-wall is directly exposed to a smaller fire, for example representing a fire in adjacent vegetation, garbage cans or similar, can be of importance. The VTT experiments of Kokkala et al [39] are taken to represent this matter.

The following chapter will present comparisons between experimental test data and results from simulations using SOFIE. The variables used for comparison are the gas temperature, surface temperature and the heat flux towards the surface at various locations on the test rig.

The uncertainty and the influence of variable fluctuations in the test data have been evaluated. Also, predicted temperatures do not include any correction term for thermocouple inertia and no radiation effects on the thermocouples have been considered, the predictions may therefore include a following, slight, deviation.

6.1 SP-fire 105 calibration test

The experimental data from these experiments are scarce due to the fact that the numbers of measurements are minimal. The measurements are made at single points and the distribution is only visually determined in terms of discoloured and charred areas. The available measurements for the calibration test that has been simulated are:

- ✓ One heat flux meter positioned at the centre of the lower window,
- ✓ Two thermocouples for assessment of temperature are positioned under the eave at different distances from the facade.

The simulations were carried out using the RHR-time chart obtained from SP. This rate of heat release is measured with a sampling hood and using the oxygen consumption calorimetry, its accuracy must be questioned. A better and a lot more accurate way to determine the heat release would be to use load cells placed under the heptane fuel tray. In this way the instantaneous mass loss is obtained and can easily be recalculated to an effective rate of heat release. While this matter is investigated further the results presented in this section must be viewed as being of preliminary kind. The chart was time adjusted slightly in order to take account for delays present when using the oxygen consumption method for RHR estimations.

Simulations are presented using the DTRM with 16 and 64 rays respectively. In the latter simulation a symmetry boundary was applied so that only half the test rig required discretisation, also a slightly finer mesh was used here. The production of soot was accounted for by a prescribed source of 2%. This may have been a somewhat too low estimate of the soot production for this particular case.

Approximately 320000 and 170000 control volumes were used for the simulations and the time required to obtain a ten-minute simulation was, in the latter case, about four weeks using an ordinary PC. The input files to SOFIE are presented in Appendix C.

Figure 6.1 shows a comparison between computed and measured temperature rise under the eave at a distance of 0.10 meters from the facade surface. The predictions are within the margin of uncertainty for both simulations. Using the larger number of prescribed rays in the calculations results in a more smooth distribution.

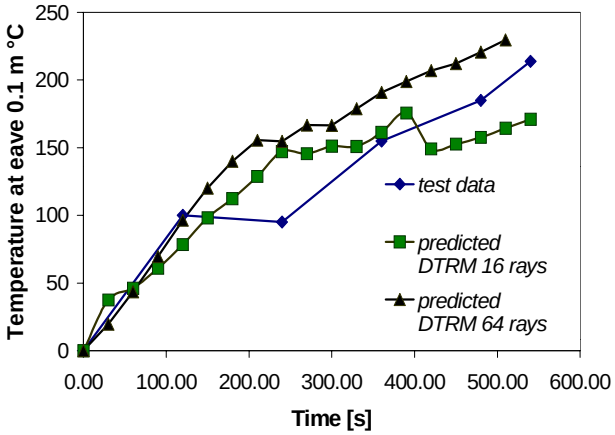

Figure 6.1 Comparison of predicted and measured temperatures at a distance 0.1 meters from facade under the eave.

It can be noted that the rise temperature is slightly over predicted compared to the test data. This tendency is also present at the edge of the eave, illustrated in figure 6.2.

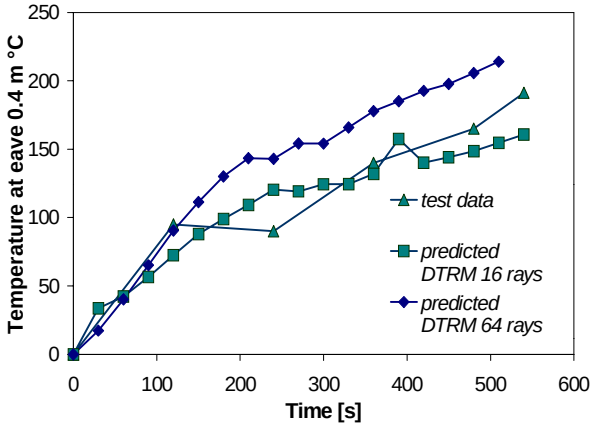

Figure 6.2 Comparison of predicted and measured temperatures at a distance 0.4 meters from facade under the eave. DTRM 64 rays.

Figure 6.3 shows the predicted total incident heat flux, using the DTRM model with 64 rays, as compared to test data.

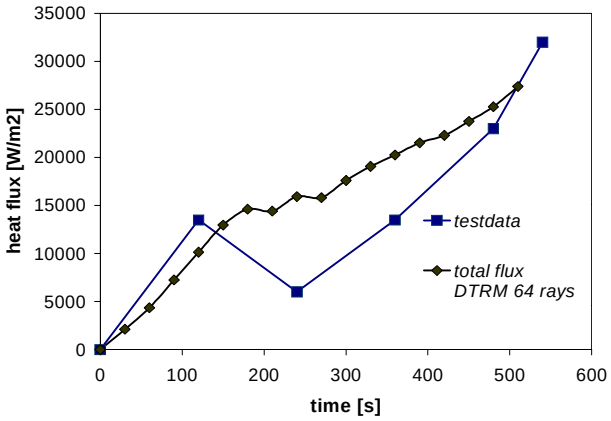

Figure 6.3 Comparison of predicted (from DTRM) and measured history of incident radiative heat flux to the lower fictious window.

The overall error in figure 6.3, for the first 500 seconds, is about 30%. Again, it is worth pointing out that the fluctuations of the dependent variable can be considerable in both time and space. In figure 6.4 iso-contours of gas temperature near the lower window is presented. Clearly, the exact position of measurement is an important issue in evaluating the results.

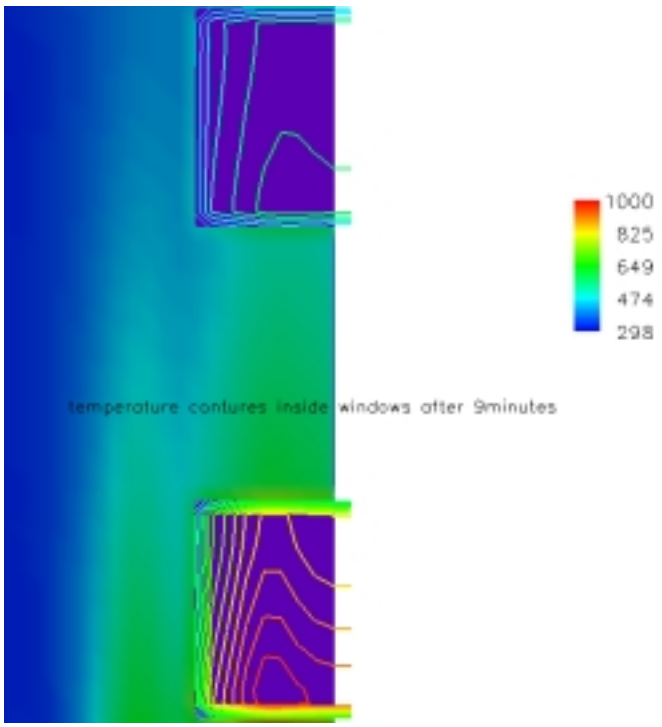

Figure 6.4 Iso contours of temperature in upper and lower windows. In the lower window the temperature in a central profile varies around 1000-800 °C.

6.2 The VTT intermediate-scale experiments

This series of tests were carried out by Kokkala et al [39] as part of their flame spread modelling efforts. Again, in this work we focus on the calibration tests, ie the experiments using non-combustible surface material. In the test presented below a calcium silicate board was used with a backing board made of mineral wool. The calcium silicate board is reported to have initial moisture content of 6-8% but this is ignored in the simulations. The burner was a line-burner using propane as fuel and the rate of heat release in the simulated experiments was 100 kW. From the photographs provided it could be seen that the flame at 100 kW is not homogenous or well defined.

These test series consists of a very large amount of data and only a selected part of these are represented in this report. The simulations used a relatively fine resolution with control volumes having a side of approximately 0.04 meters. The discrete transfer radiation model was used with 16, 64, 128 and 256 rays respectively, radiative gas properties was calculated using a discrete band weight sum of grey gases model and soot was accounted for by a prescribed source of 2 %. This value is probably slightly to low considering the soot presence in the upper parts of the flame. An additional simulation was made in which the number of control volumes was increased by a factor close to 3 and where 128 rays were used. Sample input files used in simulation are found in Appendix D.

Figure 6.5 shows predicted to experimental results of material surface temperature. In this figure two separate experimental curves are presented. These actually represent a temperature time history at the same location albeit at different sides of the centreline, thus characterising the skewness present in the experiment. The predicted values are from the simulation using a very fine mesh and 128 rays in the DT radiation model.

Figure 6.6 compares the four calculated results to the experimental data. It should be pointed out that thermocouple inertia has not been accounted for throughout the simulations. A perceptible but slight difference is noticeable. The difference between using 128 and 256 rays in the DT radiation model is extremely small. The best result is obtained for the simulation in which the number of control volumes is increased by a factor of three and the worst result is given by using 16 rays in the DTRM.

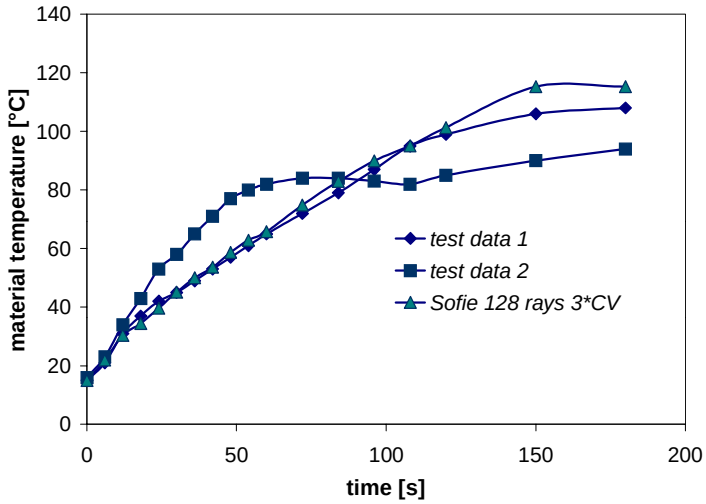

Figure 6.5 Surface temperatures on the calcium silicate board taken at a height 1.1 meter above the line-burner. The two test data is taken at the same distance from the centreline and in a perfectly symmetrical case these should coincide.

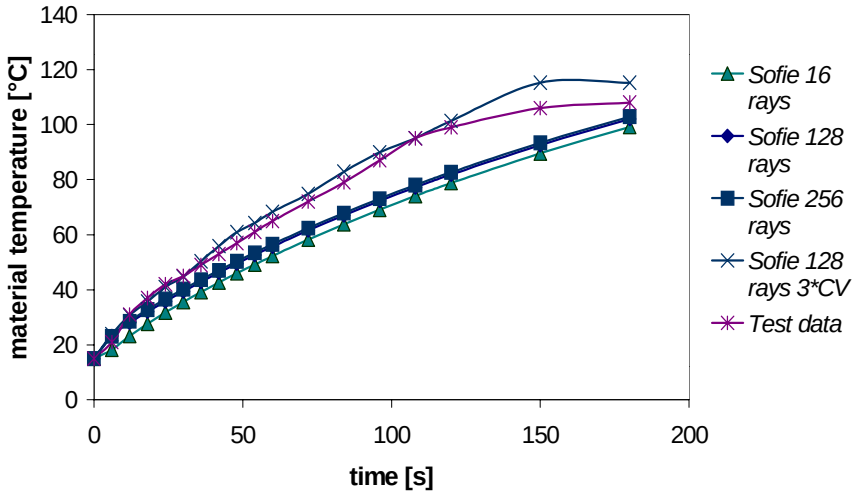

Figure 6.6 Material surface temperature time histories at about 1.1 meters above the burner. The difference in gas phase temperature is very small between simulations using the same mesh. For the finer mesh (using about 3 times the original set of control volumes) the temperature prediction is slightly more consistent with the experimental results.

Figures 6.7, 6.8 and 6.9 show comparisons between some predicted and experimental results of gas phase temperature. Simulation data in figures 6.7 and 6.8 are from simulation using 128 rays and a dense nodegrid. The difference between the predicted results becomes somewhat more distinct in the gas phase as can be seen in the figures. Still the predictions are good and can be said to fall within the margin of error. The early discrepancies in figures 6.7 and 6.9 can to some extent be attributed to time constants within the thermocouples and also to the burner.

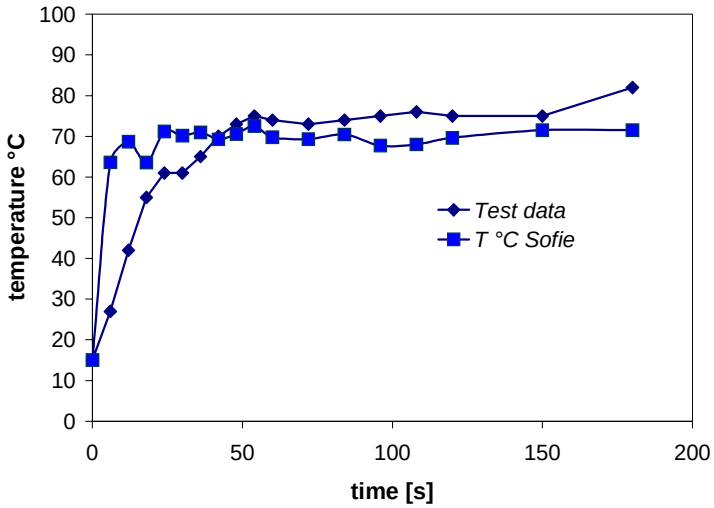

Figure 6.7 Predicted and measured gas phase temperature history 2.1 meters above the burner and some distance from the test sample.

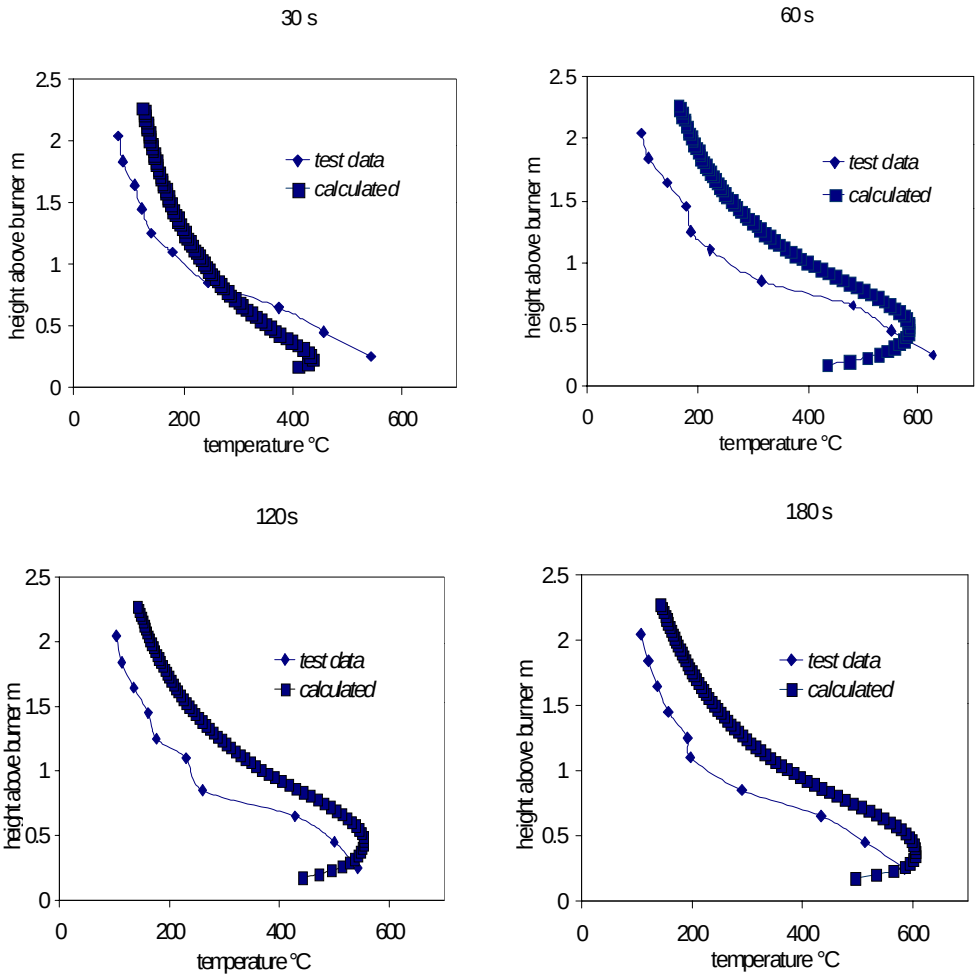

Figure 6.8 Predicted and measured gas phase temperature along the centreline for different times.

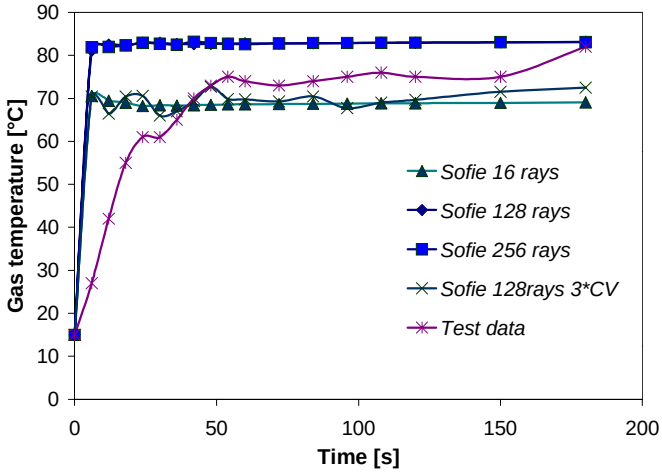

Figure 6.9 Gas temperatures 2.1 meters above the burner.

Figure 6.10 picture the steep gradients and consequently the importance of location as it shows the vertical profiles from two neighbouring rows of control volumes compared to test data. It is clear that the node location and spacing is of considerable importance.

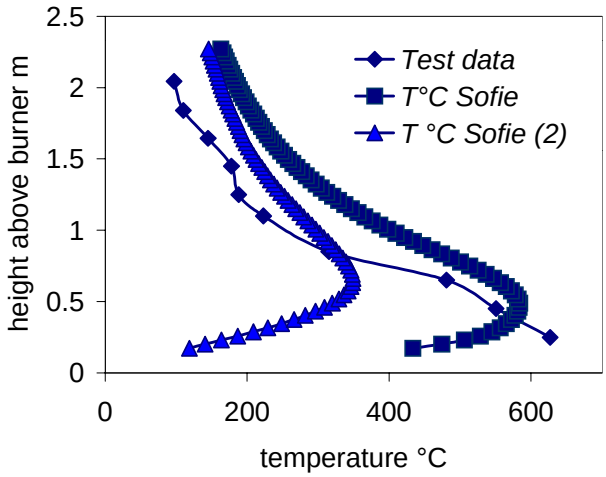

Figure 6.10 Gas-temperature distribution close to the calcium silicate board. Two predicted datasets from neighbouring vertical lines of control volumes in the simulation is presented illustrating the large gradients involved and the importance of precise knowledge of measurement positions.

Figures 6.11 and 6.12 below show predicted values of incident total heat flux compared to experimental data. The calculations using DTRM does result in underprediction of the total flux for all cases simulated but the higher the number of rays the better prediction is obtained. Also, it has been noted the DT radiation model needs to be addressed several times every time step in order to give sound predictions. This is crucial, as it may be difficult to see whether the radiation solution frequency is adequate or not only from monitoring the residual values.

The use of only 16 rays is not generally considered to yield acceptable results. Generally, a less number of rays result in a more obvious ray effect but the numerical predictions shown here is still rather satisfying considering that the testing group, reference [39], reports an accuracy not better than 15 % for the experimental data on heat flux.

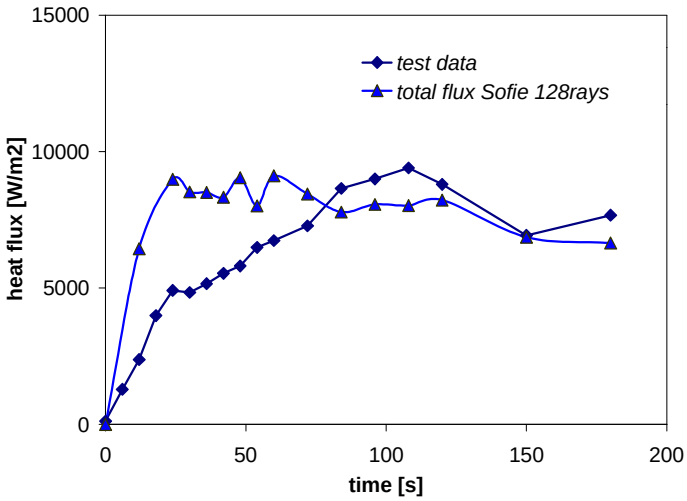

Figure 6.11 Total heat flux predicted using DTRM 128 prescribed rays and test data at approximately 1.1 meters above the burner.

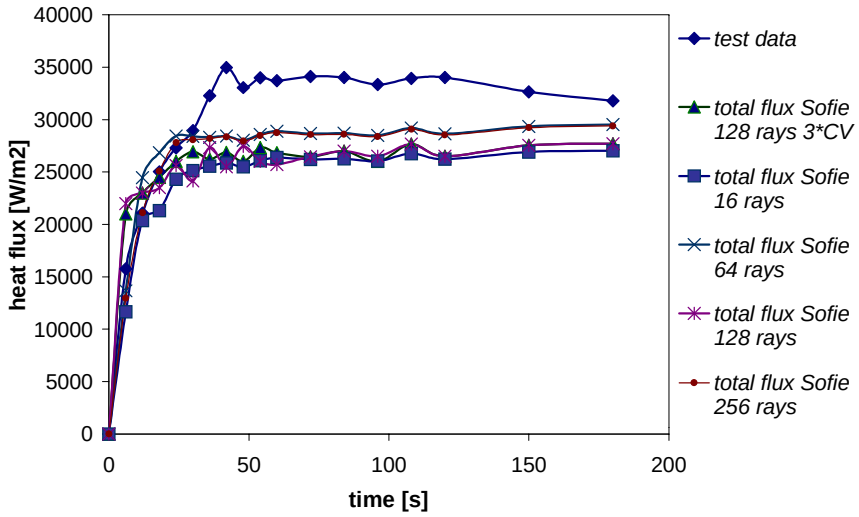

Figure 6.12 Radiative heat flux predicted using DTRM with 16, 64, 128 (2 different grid representations) and 256 prescribed rays as compared to test data 0.25 meters above the burner. Approximately 20% of the total heat flux originates from convective heat transfer.

6.3 Summary and conclusion

Two different experimental series have been simulated; one large scale represented by the SP Fire 105 and one intermediate scale taken from a series of test of Kokkala et al [39]. The focus has been on heat flux, the performance of the discrete transfer radiation model (DTRM) and its influence on dependent variables for different number of prescribed rays. The results are generally within the margin of error or can be physically or computationally predicted beforehand. The prescribed number of rays used within the DT radiation model has been shown to have a certain effect on the predicted turbulent reacting flow, primarily on gas phase variables. Nevertheless there seem to be an upper limit where its importance becomes less vital for the overall result. Using as few as 16 rays will result in an increased ray effect but in these cases the final result did not differ much from those using very many rays. As the fires in the considered scenarios can be viewed upon as being rather homogenous in width the overall ray effect is small.

In order to take further steps towards engineering methods for predicting flame spread and fire growth on facades it is necessary to closely inspect numerical results obtained from these calibration simulations. A too small number of prescribed rays may result in an inherent error as will the use of a too crude computational grid. The recommendation for future work is to use 64 rays in the DT radiation model. Using 16 rays saves considerable amount of time, but may result in errors, using 128 rays or more only cost time without improving computational results.

Finally, it is indisputable that the use of CFD techniques is the most accurate way to proceed in flame spread and fire growth modelling, independent of whether the model is purely thermal or built upon first principles.

7. A first scheme for fire safety design

The building code restrictions related to facade claddings originate from the necessity to prevent vertical spread of fire between windows in different compartments and also to minimise consequences from exposure of an outdoor fire. The heat flux towards a window one storey above a post-flashover fire will be very high independent on the actual facade material. Typically the heat flux is about 70-80 kW/m^2 for a non-combustible facade material, implying an intermediate flame exposure. This is also the limit flux determined by the building regulations.

In order to allow a more performance-based view on facade material in multi-storey buildings a methodology need to be established and a new toolkit available for engineers and architects has to be developed.

As a first step towards performance-based design solutions is to consider an equivalent to the flow-charts used in fire safety design of interior surface linings. Thus, a distinction between three different approaches is suggested here using different methods and different design criteria. Also, depending on the specific design method a safety factor has to be included.

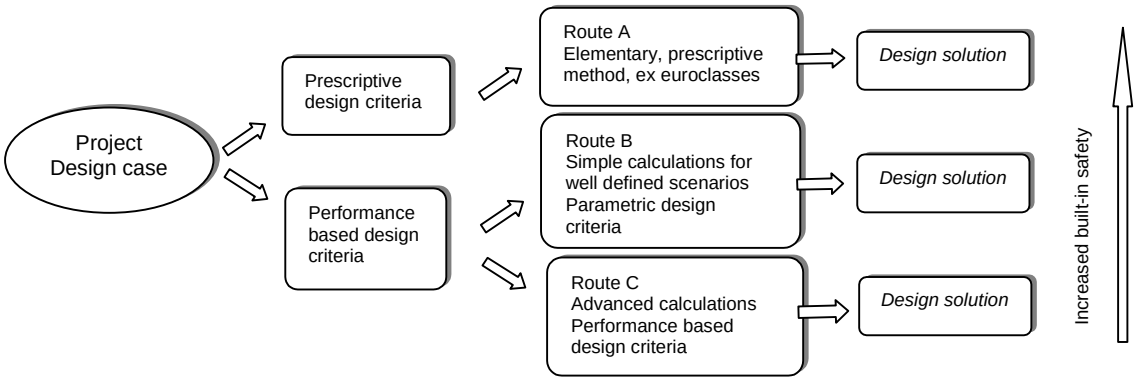

Figure 7.1 Flow-chart for the implementation of performance-based design in the construction of multi-storey facades.

The different routes, or levels of design, will have different purposes and as the simple prescriptive solution need to be very general; this level will require a relatively large predetermined safety factor.

8. References

[1] Boverkets byggregler, BBR med ändringar tom BFS 1997:

[2] Boverkets Allmänna råd 1993:2.

[3] External wall assemblies and facade claddings – Reaction to fire, SP FIRE 105, Swedish National Testing and Research Institute-Fire technology, Borås 1985 Rev: 1994.

[4] Ondrus J., Pettersson O., "Brandrisker – Utvändigt tilläggsisolerade fasader – En experimentserie i fullscala. Fire hazards of facades with externally applied additional thermal isolation – Full scale experiments", Report, LUTVDG/(TVBB-3025), Lund Institute of Technology, Lund 1986.

[5] Östman B. et al, "Brandsäkra trähus- Kunskapsöversikt och vägledning för lättbyggsystem i Norden", Byggforsk rapport O 7966, LTH rapport 3108, 1999.

[6] Hakkarinen T., Oksanen T., Mikkola E., "Fire behaviour of facades in multi storey wood framed houses", VTT Research Notes 1823, Espoo, 1997.

[7] Kuo Kenneth Kuan-yun, "Principles of Combustion", John Wiley & Sons, New York, 1986.

[8] Tuovinen Heimo, "Simulation of Combustion and Fire-Induced Flows in Enclosures", Phd thesis, Lund University, Lund, 1995.

[9] Magnussen Bjørn F., "The Eddy Dissipation Concept", subtask 3.1.C, Presented at Task Leaders Meeting, Lund, 1989.

[10] Stanisic, M. M., "The Mathematical Theory of Turbulence", Second Edition, ISBN 0-387-96685-4, Springer-Verlag- New York Berlin Heidelberg, Harrysonburg, Virginia, 1988.

[11] Abbott Michael Barry, Basco D.R., "Computational Fluid Dynamics- An Introduction for Engineers", Harlow Longman Science, 1989.

[12] Kotake Susumu, Hijikata Kunio, "Numerical Simulation of Heat Transfer and Fluid Flow on a Personal Computer", Elsevier Science Publishers B.V., Amsterdam, 1993.

[13] Versteeg H. K., Malalaselera W., "An introduction to Computational Fluid Dynamics- The finite Volume Method", Longman Scientific & Technical, Loughborough, ISBN 0-470-23515-5, 1995.

[14] Rubini, P., "SOFIE- User guide", School of Mechanical Engineering, Cranfield University, England.

[15] Kotake Susumu, Hijikata Kunio, "Numerical Simulation of Heat Transfer and Fluid Flow on a Personal Computer", Elsevier Science Publishers B.V., Amsterdam, 1993.

[16] Cox Geoffrey, "Combustion Fundamentals of Fire - Basic Considerations", Chapter 1 pp 1-30, Academic Press Ltd, London, 1995.

[17] Yan, Z., Holmstedt GA Two-Equation Turbulence Model and Its Application to a Buoyant Diffusion Flame", International J. of Heat and Mass Transfer, 42:1305-1315, 1999.

[18] Yan Z., Holmstedt G., "Fast, narrow-band computer model for radiation calculations", Numerical Heat Transfer, Part B, 31:61-71, 1997.

[19] Lewis, M.J, Moss, M.B., Rubini, P.A., "CFD Modelling of Combustion and Heat Transfer in Compartment Fires", Fire safety science, Proceedings of the fifth international symposium, pp. 463-474.

[20] Lockwood F. C., Shah N. G., "A new radiation solution method for incorporation in general combustion prediction procedures", Eighteenth Symposium (International) on Combustion, pp. 1405-1414, The Combustion Institute, Pittsburgh, PA, 1981.

[21] Glassman, Irvin, "Combustion", Third Edition, Academic Press Inc., San Diego, ISBN 0-12-285852-2, 1996.

[22] Spalding, D. B., "Mixing and Chemical Reaction in Steady Confined Turbulent Flames", Thirteenth Symposium (International) on Combustion, pp 649-657, The Combustion Institute, Pittsbourgh, PA, 1971.

[23] Kanury A. M., "Flaming ignition of solid fuels", The SFPE Handbook of Fire Protection Engineering, 2nd Edition, Section 2 Chapter 13, 1995.

[24] Niioka T., Takahashi M., Izumikawa M., 18th Symposium (Int.) Combustion, p741, 1981.

[25] Fernandez-Pello A. C., "Combustion Fundamentals of Fire - The Solid Phase", Chapter 2 pp 31-100, Editor G. Cox, Academic Press Ltd, London, 1995.

[26] Quintere J. G., "Surface Flame Spread", The SFPE Handbook of Fire Protection Engineering, 2nd Edition, Section 2 Chapter 14, 1995.

[27] Hasemi Y, "Thermal modeling of upward wall flame spread, *Fire Safety Science*, Proceedings of the First International Symposium, Hemishpere Pub. Co., 1986.

[28] Delichatsios M M, Mathews, M K and Delichatsios M A, "An upward flame spread and growth simulation" *Fire Safety Science*, Proceedings of the Third International Symposium, Elsevier Science Publishers Ltd., 1991.

[29] Beyler C L, Hunt S P, Ibqal N and Williams F W, "A computer model of upward flame spread on vertical surfaces", *Fire Safety Science*, Proceedings of the Fifth International Symposium, Melbourne, 1997.

[30] Saito K, Quintiere J G and Williams F A, "Upward Turbulent Flame Spread" *Fire Safety Science*, Proceedings of the First International Symposium, Hemisphere Pub. Co., 1986.

[31] Thomas P H and Karlsson B, "On Upward Flame Spread on Thick Fuels", SE-LUTVDG/TVBB-3058, Department of Fire Safety Engineering, Lund University, 1990.

[32] Karlsson B, ”Modelling Fire Growth on Combustible Lining Materials in Enclosures”, Report TVBB 1009, Department of Fire Safety Engineering, Lund University, 1992.

[33] Cleary T and Quintiere J G, "A framework for utilizing fire property tests", *Fire Safety Science*, Proceedings of the Third International Symposium, Elsevier Science Publishers Ltd., 1991.

[34] Baroudi D and Kokkala M, "Analysis of Upward Flame Spread", VTT Publications 89, VTT, Espoo, Finland 1992.

[35] Kokkala M and Baroudi D, ”Upward Flame Spread and Heat Release Rate of Wood Products: Experiments and Numerical Modelling”, *Fire Safety Science*, Proceedings of the Fifth International Symposium, Melbourne, 1997.

[36] Karlsson B, "Models for calculating flame spread on wall lining materials and the resulting heat release rate in a room," *Fire Safety Journal*, 1994, **23** (4) 365-386.

[37] Sundström B, "Full scale fire testing of surface materials", SP-Rapp 1986:45, SP, Borås, Sweden, 1986.

[38] Proceedings of the International EUREFIC Seminar, Copenhagen 11-12 September 1991, Interscience Communications Limited, London, 1991.

[39] Kokkala M., et al, “Large-scale upward flame spread tests on wood products”, VTT Research Notes 1834, VTT, Espoo, Finland 1997.

[40] Yan, Z., Holmstedt G., “CFD and Experimental Studies of Room Fire Growth on wall lining Materials”, Fire Safety Journal, 27, pp 201-238, 1996.

[41] Yan, Z., Holmstedt G., “CFD Simulation of Upward Flame Spread over Fuel Surface”, *Fire Safety Science*, Proceedings of the Fifth International Symposium, Melbourne, 1997.

[42] Yan, Z.,“Numerical Modeling of Turbulent Combustion and Flame Spread”, PhD thesis, Lund University, 1999.

[43] Tuovinen H, Van Hees P, Axelsson J and Karlsson B, "Implementation of a physical flame spread model in the SOFIE CFD model", SP-Report 1999:32, SP, Borås, Sweden, 1999.

[44] Lewis M J, Moss J B and Rubini P A, "CFD modelling of combustion and heat transfer in compartment fires". *Fire Safety Science*, Proceedings of the Fifth International Symposium, Melbourne, 1997.

[45] Aksit M., Mackie P., and Rubini P A, "Coupled radiative heat transfer and flame spread simulation in a compartment”, Presented at the 3rd International Seminar on Fire and Explosion Hazards, 10-14th April 2000, Lake Windermere, UK.

[46] Sibulkin M., “Heat of gasification for Pyrolysis of Charring Materials”, Fire Safety Science – Proceedings of the First International Symposium, pp 391-400, 1985.

[47] SOFIE homepage, http://www.cranfield.ac.uk/sme/sofie

Appendix A

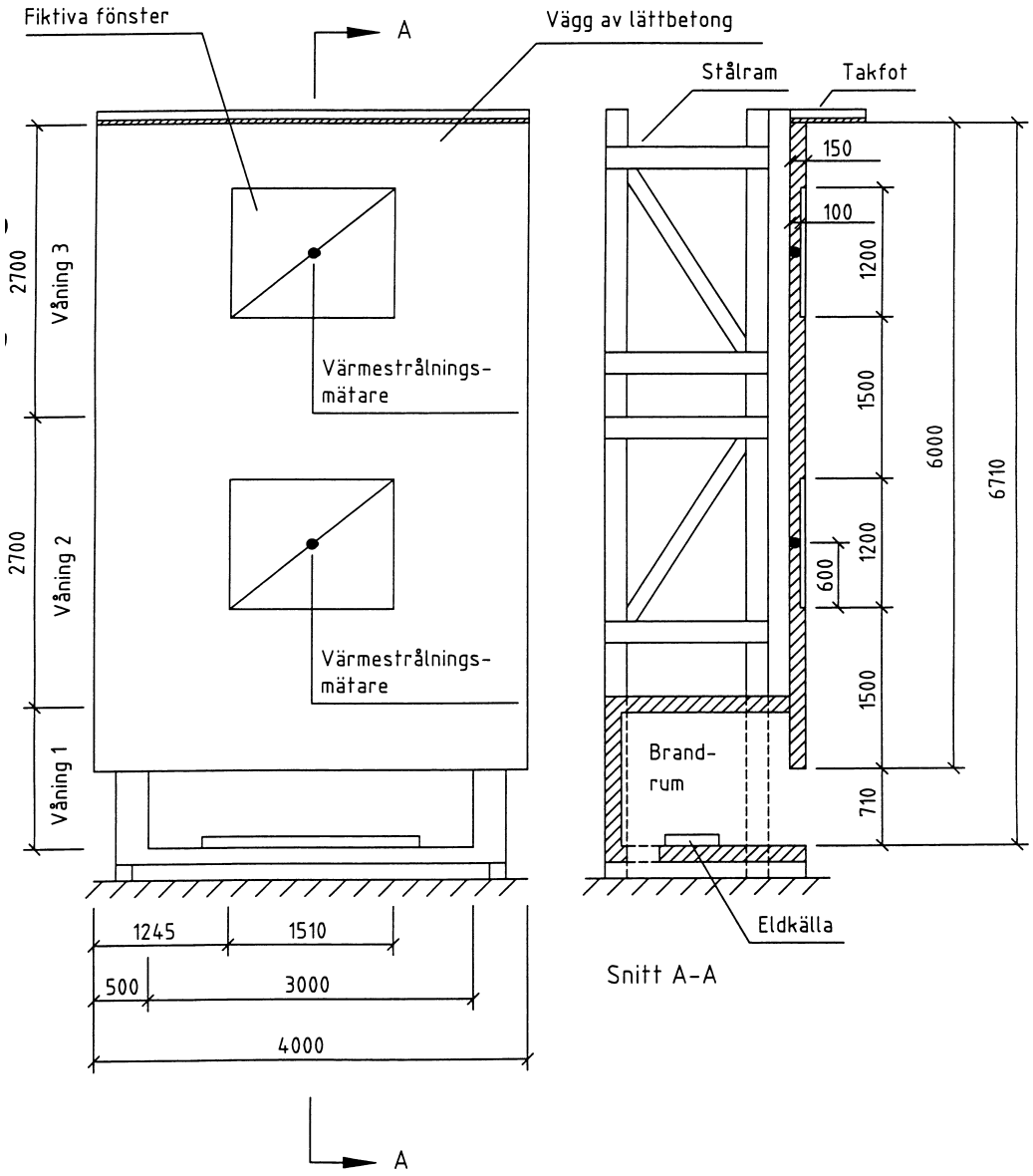

The SP-fire 105 test rig. From SP with permisson.

Appendix B

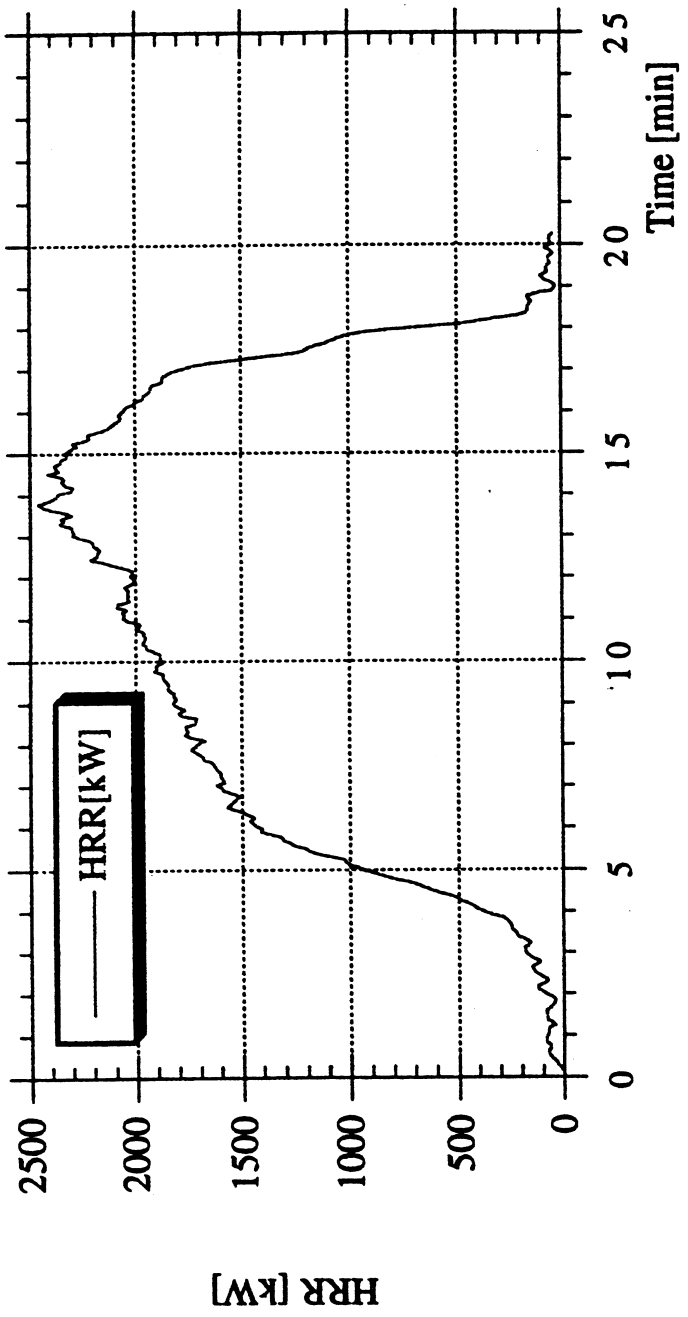

The measured rate of heat release from compartment fire as function of time. From SP with permission.

Appendix C

```
%SP Fire 105 non-combustible
%filename: sp4.com
%last modified 000526
%
%-----------------------------------------
file p p c:\sofieny\bin
opt p d p c:\sofie\database
end end
%
%@echo on
%
setup
sol type
radiation
options
RTE sol meth dis band wsgg
end
number of rays
theta dir 4
phi dir 16
end end
combustion
eddy breakup
high-Re k-e
options
buoyancy corr
SGDH
end end
fuel type
c7h16
end end
solids
add light-weight-concrete
end
passive scalar
add xgas xgas_f
end
soot
presc source
end
buoyancy
transient
species
HC comb
flamesheet
end end
%
physical geometry
import vrml
$facade1.wrl
geometr tolerance 0.01
end
%
computational grid
cartesian
key points
select object
3d object
facade
```

```
Geometry tolerance 0.01
end end
auto mesh1d
Key point tolerance 0.01
Total number of cells 200000
Minimum cells per region 2
%
modify mesh1d
x
xl_block
Number of cells 3 %0.55
Weight 1.0
xl_westwall
Number of cells 3 %0.44
Weight 1.0
xl_topwall
Number of cells 2 %0.18
Weight 1.0
xl_burner
Number of cells 3 %0.3
Weight 1.0
xh_burner
Number of cells 6 %0.5
Weight 1.0
xh_block
Number of cells 4 %0.37
Weight 1.0
xl_facade
Number of cells 5 %0.43
Weight 1.0
xh_uwindow
Number of cells 2 %0.1
Weight 1.0
xh_facade
Number of cells 2 %0.05 NOTE!
Weight 1.0
xh_eave
Number of cells 6 %0.5
Weight 1.0
xh_northb
Number of cells 25
Weight 7
end
y
yl_westwall
Number of cells 2 %0.2
Weight 1.0
yl_burner
Number of cells 2 %0.19
Weight 1.0
yh_burner
Number of cells 2 %0.1
Weight 1.0
yh_sidewall
Number of cells 6 %0.61
Weight 1.0
yl_ceiling
Number of cells 6 %0.59
Weight 1.0
yh_westwall
Number of cells 2 %0.2
Weight 1.0
```

```
yl_block
Number of cells 7 %0.71
Weight 1.0
y0036_facade
Number of cells 15 %1.2
Weight 1.0
yl_uwindow
Number of cells 15 %1.5
Weight 1.0
yh_uwindow
Number of cells 15 %1.2
Weight 1.0
yh_block
Number of cells 2 %0.2
Weight 1.0
yh_facade
Number of cells 5 %0.4
Weight 1.0
yh_eave
Number of cells 2 %0.08
Weight 1.0
yh_mirrorb
Number of cells 10
Weight 6.0
end
z
zh_lwindow
Number of cells 8 %0.76
Weight 1.0
zh_burner
Number of cells 3 %0.24
Weight 1.0
zl_sidewall
Number of cells 5 %0.5
Weight 1.0
zh_floor
Number of cells 2 %0.12
Weight 1.0
zh_westwall
Number of cells 2 %0.2
Weight 1.0
zh_eave
Number of cells 2 %0.18
Weight 1.0
zh_northb
Number of cells 5 %0.5
Weight 1.0
end end
generate mesh3d
end end
%
assign blockages
geometry
inactive burner
inactive block
active facade
active sidewall
active ceiling
active floor
active westwall
active topwall
active eave
```

```
active uwindow
active lwindow
end end
%
surface groups
geometry
create fire burner_i
create boundary_east espb
create boundary_west westb
create mirror mirrorb
%
create outer_walls westwall_o
append outer_walls topwall_o
%
create floor_ceilingo floor_o
append floor_ceilingo ceiling_o
%
create inner_walls westwall_i
append inner_walls topwall_i
%
create floor_ceilingi floor_i
append floor_ceilingi ceiling_i
%
%this is for fv only
create facade facade
create ew westwall_e
create et topwall_e
create uwindow uwindow
create lwindow lwindow
create ec ceiling_e
create ef floor_e
create eave eave
create burner burner_e
create sidewall sidewall
end end
%
boundary types
fluid inflow fire
fluid staticp boundary_east
fluid staticp boundary_west
fluid mirror mirror
end
%
boundary values
fire
v_f 0.004
t_f 371.55 %98.4 °C
mfrac_f 1.0
mfuel_f 1.0
tke_f 2.0 %percent intencity
ted_f 0.4 %lenth scale meters
sootm 0.02 %mass fraction soot
xgas 1.0 %passive scalar test
end
boundary_east
t_f 298.15
tke_f 1.0
ted_f 0.2
end
boundary_west
t_f 298.15
tke_f 1.0
```

```
ted_f 0.2
end
expert
eps_f
all_faces all_ijk ok 0.9
end end
%
interior values
expert
solution u fluid all ok -0.005
solution v fluid all ok 0.005
derived t fluid all ok 298.15
end end
%
control
s v re
enth 1.0
mfrac 0.7
mfuel 0.7
u 0.3 v 0.3 w 0.3
end
solver
enth sip
u sip
v sip
w sip
end
cycle
enth 10
end end
solver control
p c c 40
m t i 50
%
minimum residual 1e-3
%
end
phys model
time step 0.5
ambient temperature 298.15
end
rad setup n r i 1 s f 100
end end end
```

Appendix D

```
%*************************************************************
%VTT intermediate scale experiments:                          *
%Non-combustible backing no cladding  DTRM 128 rays            *
%000518                                                       *
%filename: vtt02.com                                          *
%*************************************************************
@echo on
setup
sol type
rad
op
RTE sol meth dis band wsgg
end
num o rays
theta dir 8
phi dir 16
end end
comb
eddy breakup
high-Re k-e
op
buoyancy corrections
SGDH
end end
fuel type
C3H8
end end
solids
add min-ull
add gips
end
passive scalar
add xpass xpass_f
end
soot
presc source
end
buoyancy
transient
species
HC comb
flamesheet
end
%
end
%
phys geometry
im vrml
$vtt01.wrl
geo tolerance 0.01
end
%
comp grid
cartesian
%key points
%sel obje
%3d object "something"
%Geometry tolerance 0.01
%end end
```

```
auto mesh1d
Key point tolerance 0.01
Total number of cells 70000
Minimum cells per region 2
%
modify mesh1d
%
x
xh_backing
Number of cells 2 %0.05
Weight 1.0
xl_burner
Number of cells 2 %0.02
Weight 1.0
xh_burner
Number of cells 3 %0.1
Weight 1.0
xh_beu
Number of cells 22 %1.12
Weight 6
end
y
yh_burner
Number of cells 2 %0.01
Weight 1.0
yl_beu
Number of cells 48 %1.9
Weight 1.0
yh_bwl
Number of cells 10 %0.4
Weight 1.0
yh_bn
Number of cells 12 %0.6
Weight 6
end
z
zh_backing
Number of cells 15 %0.6
Weight 1.0
zh_bwu
Number of cells 8 %0.4
Weight 1.0
end end
%
generate mesh
end end
%
assign blockages
%
geometry
inactive burner
sol typ min-ull
active backing
sol typ gips
active lining
end end
%
surface groups
geometry
create fire burner_i
create boundary_north bn
```

```
create boundary_east bel
%create boundary_westu bwu
%create boundary_westl bwl
create mirror mirror
%
create burner burner_e
create outer_backing backing_o
create inner_backing backing_i
create backing backing_e
create inner_lining lining_i
create outer_lining lining_o
create lining lining_e
%
end end
%
boundary type
fluid inflow fire
fluid staticp boundary_north
fluid staticp boundary_east
%fluid staticp boundary_west
fluid mirror mirror
thermal htcoef outer_backing
end
%
boundary values
fire
v_f 0.009635 %100kW
t_f 288.15
mfrac_f 1.0
mfuel_f 1.0
tke_f 3.0 %percent intencity
ted_f 0.1 %lenth scale meters increase
sootm 0.02
xpass_f 1.0
end
boundary_north
t_f 288.15
tke_f 1.0
ted_f 0.1
end
boundary_east
t_f 288.15
tke_f 1.0
ted_f 0.1
end
%boundary_westu
%t_f 288.15
%tke_f 1.0
%ted_f 0.1
%end
outer_backing
htcoef_f 7.0
end
expert
eps_f
all_faces all ok 0.9
end end
%
interior values
backing der t bl 288.15 end
lining der t bl 288.15 end
```

```
expert
solution  u    fluid  all ok -0.01
solution v  fluid  all ok 0.01
der t fluid all ok 288.15
end
end
con p m t s 0.5 amb temp 288.0 end
s c m t i 100 m r 0.01 end
s v relax
enth 1.0
mfrac 0.7
mfuel 0.7
end
cycle
enth 10
end
solver all sip
end
schem all tvd
end end
rad set
n r i 3
s f 50
end
end
end
%
@echo off
```